Molluscs in the Levantine Upper Palaeolithic: implications for modern human diets and subsistence behaviour

Bosch, D.M.

Citation

Bosch, D. M. (2018, May 3). *Molluscs in the Levantine Upper Palaeolithic: implications for modern human diets and subsistence behaviour*. Retrieved from https://hdl.handle.net/1887/61828

Cover Page

Universiteit Leiden

Author: Bosch, D.M.
Title: Molluscs in the Levantine Upper Palaeolithic: implications for modern human diets and subsistence behavior
Issue Date: 2018-05-03

Chapter 3 • New chronology for Ksâr 'Akil (Lebanon) supports Levantine route of modern human dispersal into Europe

New chronology for Ksâr 'Akil (Lebanon) supports Levantine route of modern human dispersal into Europe

Marjolein D. Bosch[a,1], Marcello A. Mannino[a], Amy L. Prendergast[b], Tamsin C. O'Connell[c], Beatrice Demarchi[d], Sheila M. Taylor[e], Laura Niven[a], Johannes van der Plicht[f,g], and Jean-Jacques Hublin[a]

[a]Department of Human Evolution, Max Planck Institute for Evolutionary Anthropology, D-04103 Leipzig, Germany; [b]Institute of Geosciences, Applied and Analytical Palaeontology, University of Mainz, D-55128 Mainz, Germany; [c]Department of Archaeology and Anthropology, University of Cambridge, Cambridge CB2 3DZ, United Kingdom; [d]BioArCh, Department of Archaeology, University of York, York YO10 5DD, United Kingdom; [e]Department of Chemistry, University of York, York YO10 5DD, United Kingdom; [f]Center for Isotope Research, Groningen University, 9747 AG Groningen, The Netherlands; and [g]Faculty of Archaeology, Leiden University, 2333 CC Leiden, The Netherlands

Modern human dispersal into Europe is thought to have occurred with the start of the Upper Paleolithic around 50,000–40,000 y ago. The Levantine corridor hypothesis suggests that modern humans from Africa spread into Europe via the Levant. Ksâr 'Akil (Lebanon), with its deeply stratified Initial (IUP) and Early (EUP) Upper Paleolithic sequence containing modern human remains, has played an important part in the debate. The latest chronology for the site, based on AMS radiocarbon dates of shell ornaments, suggests that the appearance of the Levantine IUP is later than the start of the first Upper Paleolithic in Europe, thus questioning the Levantine corridor hypothesis. Here we report a series of AMS radiocarbon dates on the marine gastropod *Phorcus turbinatus* associated with modern human remains and IUP and EUP stone tools from Ksâr 'Akil. Our results, supported by an evaluation of individual sample integrity, place the EUP layer containing the skeleton known as "Egbert" between 43,200 and 42,900 cal B.P. and the IUP-associated modern human maxilla known as "Ethelruda" before ~45,900 cal B.P. This chronology is in line with those of other Levantine IUP and EUP sites and demonstrates that the presence of modern humans associated with Upper Paleolithic toolkits in the Levant predates all modern human fossils from Europe. The age of the IUP-associated Ethelruda fossil is significant for the spread of modern humans carrying the IUP into Europe and suggests a rapid initial colonization of Europe by our species.

modern human dispersal | Upper Paleolithic | Near East | chronology | zooarcheology

Fossil and genetic evidence suggest that anatomically modern humans (AMH) originated in Africa and colonized Europe between at least 50,000–40,000 calendar years ago (cal B.P.; i.e., calendar years relative to AD 1950) (1–6). The modern human fossil record for this time period is limited to only a few remains, including those found at Ksâr 'Akil (7) and Manot Cave (8) in the eastern Mediterranean region of southwestern Asia and Peştera cu Oase in Romania (2) (*SI Appendix*, Section 3). The interpretation of this scant record is affected by imprecise chronologies, and in some cases, by problematic stratigraphies or lack of contextual data (2, 8–10). The recently discovered fossil at Manot (Israel) places AMH in the Levant as early as 60,200–49,200 y ago (8). However, because the fossil was found on a natural shelf unconnected with the otherwise rich archeological deposits elsewhere in the cave, its affiliation to an archeological technocomplex is unclear. Based on the uranium–thorium dates, the authors suggest an attribution of the fossil to either a late Middle Paleolithic (MP) or Initial Upper Paleolithic (IUP) technocomplex. The lack of archeological association and contextual behavioral data limits our understanding of the fossil's relation to both the Levantine and the European record. Hence, there is very little information to study the dispersal trajectory

of modern humans into Europe. However, bones of modern humans from the Levant (e.g., Üçağızlı I and Ksâr 'Akil) and Europe (e.g., Kostenki 1, 14, and 17) are found in archeological contexts and in association with Early UP (EUP) lithic technologies (7, 9, 11, 12). These lithic assemblages, therefore, can be used as a proxy for modern human dispersal (13) and links between several such Levantine and European technocomplexes have been documented (11, 12, 14–16). The archeological record suggests that modern human dispersal from Africa likely took place in several episodes rather than one large exodus (3, 6, 14, 17–19). This hypothesis is supported by genetic and fossil data (20).

AMH dispersal into Europe is broadly contemporaneous with the disappearance of Neanderthals and the beginning of the UP, as witnessed by changes in the archeological record including frequent use of red ochre, modified marine shells and perforated animal teeth as body ornaments, elaborate bone and antler technology, as well as changes in lithic technology (19). Most scholars (3, 6, 14, 19, 21, 22) advocate the importance of southwestern Asia, including the Levant, as a "gateway" to Eurasia for modern humans coming from Africa. This Levantine corridor hypothesis has recently been questioned, as it has been argued that the UP and modern behavior, evidenced by the presence of shell beads in the material culture, first appeared in Europe before their first occurrence in the Levant (23). This interpretation is based on a

Significance

Bayesian modeling of AMS radiocarbon dates on the marine mollusk *Phorcus turbinatus* from Ksâr 'Akil (Lebanon) indicates that the earliest presence of Upper Paleolithic (UP) modern humans in the Levant predates 45,900 cal B.P. Similarities in early UP lithic technology and material culture suggest population dispersals between the Levant and Europe around 50,000–40,000 cal B.P. Our data confirm the presence of modern humans carrying a UP toolkit in the Levant prior to any known European modern human fossils and allow rejection of recent claims that European UP modern humans predate those in the Levant. This result, in turn, suggests the Levant served as a corridor for the dispersal of modern humans out of Africa and into Eurasia.

ANTHROPOLOGY

combination of relatively old ages (around 39,900 cal B.P.) for Uluzzian ornamental shell in southern Italy (10) and strikingly young ages (around 36,300–37,400 cal B.P.) for shell ornaments from Üçağızlı I and Ksâr 'Akil in the Levant (23, 24). If the UP in Europe truly predates the Levantine evidence, as Douka et al. (24) suggest, it should be considered unlikely that its makers traveled from Africa through the Levant before arriving in Europe. Here, we provide a new chronology for Ksâr 'Akil and show that the earliest UP and its associated AMH remains predate any European evidence.

Ksâr 'Akil

Located on the Lebanese coast, Ksâr 'Akil is a key site for the region and is best known for its 23-m-long sequence, which includes rich IUP (Layers XXV–XXI) and EUP (Layers XX–XIV) deposits, both of which contain modern human remains (*SI Appendix*, Fig. S1.2). The site, about 10 km north of Beirut, lies about 3 km from the present day coast (*SI Appendix*, Section 1). Excavations conducted in the 1930s and 1940s (7, 25) exposed the entire sequence, whereas later investigations (26) did not reach the earliest UP deposits.

In Layer XXV, the lowermost part of the deposit attributed to the IUP, a maxillary fragment ("Ethelruda") was found accompanied by IUP lithics (7, 27). Ethelruda was initially interpreted as having "Neanderthaloid" features by the excavators (7), but reexamination of the fossil suggests that it falls within the range of modern human variation (28). In general, the IUP lithic assemblages are characterized by opposed platform blade cores with parallel edges and facetted platforms (29). Tool types include chamfered pieces, endscrapers, and burins (27, 29). *Dama mesopotamica* is the dominant vertebrate species throughout all IUP layers. Further, the IUP witnessed a shift in the vertebrate fauna, with a drop in the numbers of *Bos* sp. and *Sus scrofa* in favor of *Capra ibex*, *Capra aegagrus*, and *Capreolus capreolus*. Evidence for marine mollusk consumption is rare and first occurs in Layer XXII (*SI Appendix*, Section 1).

The EUP or Early Ahmarian is associated with the remains of an 8-y-old modern human ("Egbert") and possibly a second individual (25) in Layer XVII, both now lost. The classic Early Ahmarian (Layers XVIII–XVI) also features opposed platform cores with parallel edges, in this case with plain platforms and marginal flaking resulting in thinner blanks (29). Tool types include endscrapers, retouched blades, and bladelets including el-Wad points and *pointe à face plane*, whereas burins are virtually absent (29). *Dama mesopotamica* dominates the vertebrate fauna, but there is a shift to more evenly distributed numbers of *Cervus elaphus*, *Capra aegagrus*, *Capra ibex*, *Sus scrofa*, *Gazella* cf. *dorcas*, and *Testudo graeca* compared with the underlying IUP. In addition, marine intertidal gastropods increase in number and were a foodstuff consumed by the site's EUP occupants (*SI Appendix*, Section 1).

## Results

The multidisciplinary approach adopted in this study included absolute dating (AMS radiocarbon), an attempt to attribute layers to climatic events (*SI Appendix*, Section 2) using oxygen isotope analysis as a paleotemperature proxy, the use of amino acid racemization (AAR) to verify the extent of intracrystalline protein diagenesis and thus to highlight potentially compromised samples, as well as in-depth zooarcheological and taphonomic analyses. A relatively large shell assemblage ($n > 3,500$) was recovered during the 1930s and 1940s excavations mainly from the UP layers (XXIV–I) (25, 30). The shells belong to marine, terrestrial, and freshwater species from a variety of habitats (*SI Appendix*, Table S1.2). Marine shells, collected empty from active beaches or fossil deposits, were used as tools (e.g., *Glycymeris* sp.) and ornaments (e.g., *Nassarius gibbosulus* and *Columbella rustica*) (30–32). Limpets (*Patella rustica*, *Patella caerulea*, and *Patella ulyssiponensis*)

and topshells (*Phorcus turbinatus* and *Phorcus articulatus*) were live-collected for consumption and are the best-preserved taxa in the assemblage. Evidence for collection of live limpets and topshells includes the overall integrity of their shells, absence of bioerosion, and encrusting organisms on inner shell surfaces, as well as edge notches on limpet shells congruent with damage resulting from prying the animals off the rocks. Other subsistence-related anthropogenic modifications include the frequent intentional removal of the apices of *Phorcus turbinatus* to facilitate flesh extraction and occasional burning (*SI Appendix*, Section 1). By dating food remains, the "dated event" (i.e., incorporation of ^{14}C in the shell carbonate during growth) and "target event" (i.e., human foraging) directly follow each other (33). Therefore, dating *Phorcus turbinatus* shells captures a concise timeframe including mollusk collection and consumption and is thus a good proxy for site occupation. Individual shells of this species were selected based on their excellent preservation, by considering a combination of macroscopic and physicochemical characteristics (*SI Appendix*, Section 2).

Radiocarbon Dating. We obtained 16 AMS radiocarbon dates for the Ksâr 'Akil UP sequence (Layers XXII–V) (*SI Appendix*, Table S2.2). All age estimations are calibrated using the Marine13 curve (34) and are given at the 68.2% probability level (*SI Appendix*, Section 2). *Phorcus turbinatus* occurs in the IUP starting from Layer XXII, which is dated to 44,400–43,100 cal B.P. The 11 dates for the EUP (Layers XX–XVI) show a wide range of ages from 44,000–37,200 cal B.P., whereas the later UP (Layers XII, XI, and VI) dates to ~40,700–31,700 cal B.P. The start of the Epipaleolithic or Proto-Kebaran (Layer V) can be placed at 30,400–29,500 cal B.P. Artifact associations made during the 1930s and 1940s were based on broad geological layers that potentially include several thinner archeological horizons (*SI Appendix*, Section 1). This limited detail in provenience could account for wide age ranges within a layer. The dates of samples XVII (1) and XVIII do not fit well in the overall sequence because they provided younger ages than overlying samples. These specimens could be intrusive from younger deposits or be subjected to contamination. In general, contamination of a sample of this age results in a younger estimate than the true age of the sample, because the effect of introducing modern carbon in highly ^{14}C-depleted samples is more pronounced than the effect of introducing radiocarbon-dead contaminants (35, 36). The fact that the dated material comes from an old excavation with inherent provenience limitations, and the problems of identifying and eliminating contaminants in shells, make it imperative to evaluate individual sample integrity. We have applied three independent methods to evaluate our chronological data and identify potential outliers: (*i*) modeling using Bayesian statistics (37), (*ii*) using AAR values as a proxy for diagenetic integrity of the shells, and (*iii*) analyzing the oxygen isotope composition of shell carbonates to evaluate whether all specimens from the same layer are likely to be contemporary and to compare paleotemperature estimates from these analyses with those documented for different climatic phases in the NGRIP curve (*SI Appendix*, Section 2).

Bayesian Modeling of the Radiocarbon Ages. Bayesian modeling (37) and outlier analysis resulted in a model with an agreement index (A_model) of 118.2% (Fig. 1; see *SI Appendix*, Section 2 for discussion of rejected alternative models). For six dates, high posterior outlier probabilities (indicative of outliers) were calculated at various stages of the modeling (*SI Appendix*, Table S2.4). The model identifies the older EUP dates as best reflecting the true ages. We used the OxCal "Date" function to calculate a probability distribution function (PDF) for the age of the human fossil-bearing archeological layers. The PDF for Egbert's layer results in an age of 43,200–42,900 cal B.P. Regarding the age of Ethelruda, a lack of datable material from its
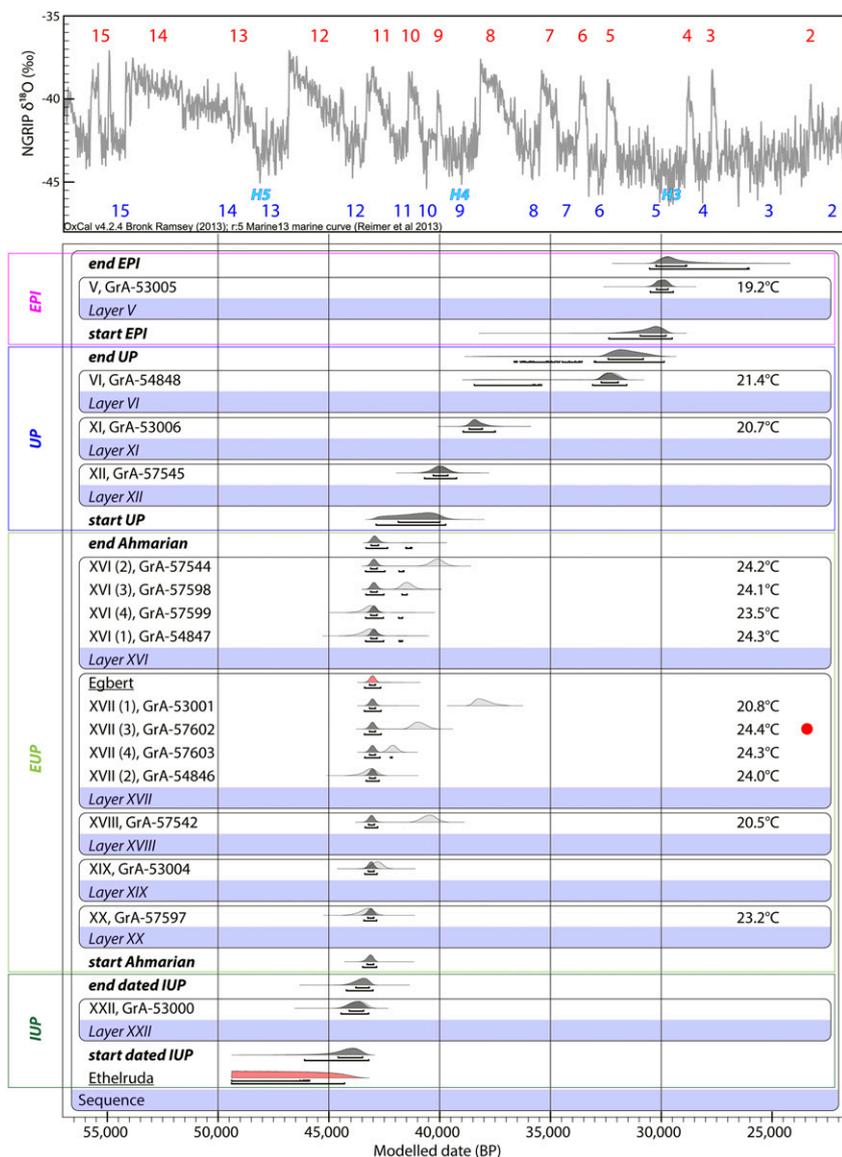
Fig. 1. Bayesian age model for the Ksâr 'Akil sequence produced using OxCal 4.2.4 (37). The radiocarbon dates are calibrated using the Marine13 dataset (34) ΔR value for the eastern Mediterranean (60). The individual radiocarbon likelihoods are shown in light gray, the posterior probability distributions are shown in dark gray, and PDFs for Ethelruda and Egbert's layers are shown in red. The modeled data are compared with the NGRIP δ¹⁸O curve (gray), Greenland Interstadials (GIS; red) and Stadials (GS; blue), and Heinrich Events (H3-5; light blue). Mean annual SSTs are given in degrees Celsius (°C). A red dot marks date XVII (3), as AAR analyses of the intracrystalline proteins showed that this sample displays some indication of open-system behavior.

associated Layer XXV, as well as from the layers directly above and underneath, hampers precise age estimation. Nevertheless, the date of the overlying IUP Layer XXII and the modeled start of the dated part of the IUP sequence provide termini ante quem for Ethelruda (i.e., >44,100 cal B.P. and >44,600 cal B.P., respectively). The PDF for Ethelruda's layer extends beyond the range of the Marine13 calibration curve, and the upper limit of 45,900 cal B.P. can be used as a minimum age.

Amino Acid Racemization (AAR). The extent of racemization (D/L value) of 26 *Phorcus turbinatus* specimens, including 13 AMS dated samples, was evaluated. Both the total hydrolysable amino acids (THAA) and free amino acids (FAA) retained in an intracrystalline protein fraction (isolated by bleaching) of several amino acids were considered (*SI Appendix*, Section 2). Overall, intralayer variability of the D/L values was found to be comparable to the intrasite variability (*SI Appendix*, Fig. S2.7), and therefore D/Ls could not be used to resolve the relative chronology within the site. However, the covariance between FAA D/Ls and THAA D/Ls of different amino acids showed that the intracrystalline proteins in *Phorcus turbinatus* provide a robust fraction for AAR analyses (closed-system behavior). This result

indicates that the shells had not been diagenetically compromised during their postdepositional history, supporting the results of the other geochemical methods and AMS dates (*SI Appendix*, Fig. S2.6). One exception is sample XVII (3), which shows some indication of open-system behavior, supporting the hypothesis that this date might be an outlier (Fig. 1).

Oxygen Isotope Analysis. δ¹⁸O values of sequential carbonate samples from 13 specimens were converted to Sea Surface Temperatures (SST) and provided mean annual SST estimates (*SI Appendix*, Section 2). Observed fluctuations in mean annual SST, of 3–4 °C, are consistent with differences between warm Greenland Interstadials (GIS) and cooler Greenland Stadials (GS), including Heinrich events during Marine Isotope Stage 3 (MIS 3) (38). Oxygen isotope and SST data are consistent with the climatic phases inferred from tentative correlations of calibrated ages with the NGRIP data (Fig. 1). These tentative comparisons allow us to attribute samples with higher δ¹⁸O$_{shell}$ values [i.e., V, VI, XI, and XVII (1), and XVIII], corresponding to SST estimates between 19.2 °C and 21.4 °C, to cold events i.e., Heinrich 3, GS 5/6, GS 9, and GS 10, respectively. Samples with lower δ¹⁸O$_{shell}$ values, corresponding to temperatures ranging from 23.2 °C to 24.4 °C,

ANTHROPOLOGY

could be attributed to GIS 11 [i.e., XVI (1), XVI (4), XVII (2), XVII (4), and XX] and GIS 10 [i.e., XVI (2, 3) and XVII (3)] (39). The colder annual SST estimate for sample XVII (1) is inconsistent with that of other Ahmarian samples, indicating that this specimen did not secrete its shell in the same temperature regime and is not contemporary with the others, which is also reflected by the younger AMS date. Provided the date is correct, this specimen is most likely intrusive from the later cold period GS 9.

Discussion

The chronological data reported above suggest that modern humans producing IUP and EUP assemblages were present at Ksâr 'Akil from before 45,900 cal B.P. and around 43,300–42,800 cal B.P., respectively. These age estimates have implications for (*i*) the chronology of the Levantine EUP and IUP, (*ii*) the age of UP modern human presence in the Levant, (*iii*) the spread of UP modern humans from the Levant into Eurasia, and (*iv*) the validity of the Levantine corridor hypothesis.

Ksâr 'Akil Chronology and Previous Dates. Our dates are in good agreement with conventional radiocarbon dates on charcoal (26, 40). They also overlap with the age estimates on shell by Douka et al. (24) for the upper part of the sequence, but are significantly older (3,000–4,000 y) for the IUP and EUP layers (*SI Appendix, Section 2*). The reasons behind the observed discrepancy are presently unresolved. Causes might include differences in (*i*) sample selection (i.e., shell preservation and its implications for time-averaging and diagenesis), (*ii*) sample pretreatment (e.g., potential incomplete elimination of contaminants by the CarDS method) (41), (*iii*) radiocarbon AMS laboratory (i.e., Groningen

and Oxford), and (*iv*) the dated event based on taxa selection (i.e., collection of beached shells for ornaments or live mollusks for consumption; see *SI Appendix, Section 2* for discussion).

Chronology in a Regional Context.

Levantine IUP chronology. The earliest IUP in the Levant is represented by Manot Cave and Boker Tachtit (both Israel), Üçağızlı I Cave (Turkey), and as inferred from Kebara Cave (Israel) (Fig. 2; *SI Appendix, Section 3*). For comparative purposes, radiocarbon dates were calibrated using IntCal/Marine13 (34) unless stated differently (*SI Appendix, Section 3*). A single AMS date from Unit 7 of Area C at Manot Cave of 48,700 [14]C B.P. is attributed to the IUP. It cannot be calibrated as it falls beyond the limits of the current calibration curve. The IUP lithics share features with Ksâr 'Akil IUP Layers XXV–XXI, but the unit also contains abundant EUP and scattered MP artifacts (8). Age calibration of conventional radiocarbon dates on charcoal suggests that the IUP at Boker Tachtit (Layers 1–4) dates to at least 50,000–40,000 cal B.P. (42), which should probably be considered a minimum estimate (43). The lithic assemblage of Layer 4 shows technological similarities with Ksâr 'Akil Layers XXII–XXI and is associated with a charcoal date of ~40,000 cal B.P., again a minimum age (42). The IUP at Üçağızlı I (Layers G–I) corresponds to Layer XXI of Ksâr 'Akil (31) and dates to 45,900–38,400 cal B.P. based on charcoal samples (9) and 40,800–37,800 cal B.P. based on shell ornaments (23). Kebara has a hiatus in the stratigraphy where the IUP would be expected to occur; based on age estimations for the Late Middle Paleolithic below and the EUP above, Rebollo et al. (44) assign a time window of 49,000–46,000 cal B.P. for the IUP. The estimated start of the IUP at Ksâr 'Akil, modeled to at least 45,900 cal B.P., is
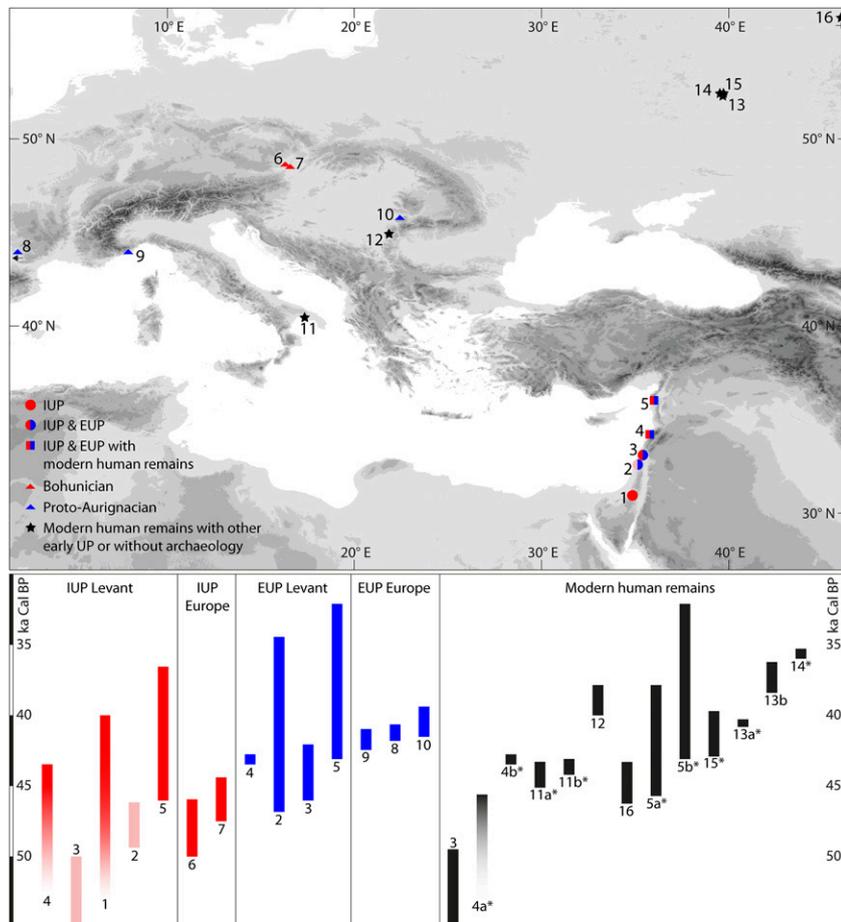
Fig. 2. Upper Paleolithic sites and human remains mentioned in the text (see also *SI Appendix, Section 3*). (*Upper*) Site location. (*Lower*) Age range (in 1,000 calendar ages before present) of sites and human remains (*: in association with UP). 1, Boker Tachtit; 2, Kebara Cave; 3, Manot Cave; 4, Ksâr 'Akil; 4a, Ethelruda; 4b, Egbert; 5, Üçağızlı I; 5a, Üçağızlı I IUP teeth; 5b, Üçağızlı I EUP teeth; 6, Brno-Bohunice 2002; 7, Brno-Kejbaly; 8, Isturitz; 9, Riparo Mochi; 10, Românești-Dumbrăvița I; 11a Cavallo B; 11b, Cavallo C; 12, Peştera cu Oase; 13a, Kostenki 14 Layer IVb tooth; 13b, Kostenki 14 Burial; 14, Kostenki 1 Layer III; 15, Kostenki 17 Layer II; 16, Ust'-Ishim.

congruent with technological and chronological data from all four sites, of which the Manot IUP might be the most ancient.

Levantine EUP chronology. Our dates agree with established chronologies for other Levantine EUP or Early Ahmarian sites including Kebara, Manot, and Üçağızlı I. The Early Ahmarian at Kebara (Units III and IV) is dated between 46,000 and 34,000 cal B.P. and corresponds archeologically to Ksâr 'Akil Layers XIX–XV (44, 45). The Early Ahmarian component of Unit 7 (Area C) at Manot has been dated to 46,000–42,000 cal B.P. (46) and corresponds to Layers XX–XVI. The EUP Layers B to B4 at Üçağızlı I, dated to 39,800–32,200 cal, are similar in lithic technology but younger than Ksâr 'Akil Layers XVI–XVII (9, 31). Age estimates for the entire EUP sequence (Layers B–E) range between 42,800 and 32,200 cal B.P. (9) and 40,800 and 36,400 cal B.P. based on shell ornaments (23). The EUP of the four sites overlaps, although its start at both Manot and Kebara predates that of Üçağızlı I and Ksâr 'Akil by several millennia.

Implications for UP Modern Human Dispersals into Europe and the Levantine Corridor Hypothesis.

AMH remains. Ksâr 'Akil is one of the few sites with AMH fossils that are associated with IUP and EUP assemblages in Europe and the Levant. Our age estimations, placing Egbert's layer between 43,200 and 42,900 cal B.P., predate directly dated AMH remains from Europe, including those from Peştera cu Oase and Kostenki 14 (Russia) (Fig. 2 and *SI Appendix*, Section 3) (2, 11, 47), and overlap at 1σ with the modeled age for Cavallo C (Italy) (10). Further, this age is consistent with those for the AMH teeth from the EUP layers of Üçağızlı I (42,800–32,200 cal B.P.) (9). Our data also provide a minimum age of at least 45,900 cal B.P. for the archeological layer bearing the remains of Ethelruda and the start of the IUP in Layer XXV, placing the fossil well before the oldest European AMH fossil (i.e., Cavallo B dated to 45,000–43,400 cal B.P., *SI Appendix*, Table S3.2) (10). In contrast to the Ust'-Ishim femur (46,200–43,700 cal B.P.) (22), the Manot 1 skull (60,200–49,200 y ago) (8) might predate the IUP at Ksâr 'Akil. However, the uranium–thorium age of the latter is rather imprecise and none of these specimens was found in direct archeological context. It is therefore unclear what toolkit these humans carried. Within the Levant, the Ksâr 'Akil data are in rather good agreement with the age estimations for Üçağızlı I, where AMH teeth from the IUP date between 45,900 and 37,100 cal B.P. (9). Compared with European modern human remains associated with UP toolkits, the Ksâr 'Akil data predate the human remains from early UP contexts at Kostenki 14 Layer IVb between 41,500 and 40,900 cal B.P. (11, 48) and at Kostenki 17 Layer II dated to 42,800–39,600 cal B.P. (12) (*SI Appendix*, Section 3).

Archeological record. Similarities between Levantine and European early UP technocomplexes have been interpreted as evidence of several dispersal episodes (3, 6, 14, 18, 19). The earliest connection concerns the Levantine IUP/Emirian and Central European Bohunician and similar assemblages in Eastern Europe and North Asia (11, 14, 15, 21, 49). Similarities have also been documented between the Levantine Early Ahmarian (EUP) and the European Proto-Aurignacian (3, 16, 19, 50, 51). Therefore, identifying the first occurrence of technologically similar lithic industries in the Levant and Europe holds potential information about dispersal trajectories. In the case of the Levantine IUP and European Bohunician connection, the latter is generally placed in GIS 12 (21, 52) with its onset around 46,860 ± 956 b2k (i.e., calendar years before A.D. 2000) (39), or in GIS 13 (53). The estimated start of the IUP at Ksâr 'Akil falls within GIS 12, but could also predate it. The dates of Boker Tachtit and Manot predate GIS 12, and could be as early as GIS 13 and GIS 14, respectively. The start of the Levantine EUP at Ksâr 'Akil, Kebara, and Manot predates the appearance of the Proto-Aurignacian in Europe around 42,700–39,100 cal B.P., i.e., at Isturitz (54), Riparo Mochi (55) and Românești-Dumbrăvița I (56), by several millennia (*SI Appendix*, Section 3).

Implications. On an interregional scale, similar UP lithic technocomplexes (e.g., IUP/Bohunician and Early Ahmarian/Proto-Aurignacian) first appear in the Levant. Our chronology for Ksâr 'Akil, corroborated by several lines of evidence, fits well with other early IUP and EUP Levantine sites. It is generally assumed that once there is a proven association between certain archeological assemblages and their makers, this could be extrapolated to the technocomplex as a whole (e.g., all Early Ahmarian is made by modern humans based on association of the Egbert fossil to the Ksâr 'Akil EUP). Although such extrapolations should be treated with caution especially when they are extended to other closely related assemblages over a large geographical area, the correlation of AMH associated technocomplexes with other closely related technocomplexes allows tracking of potential dispersal routes in the archeological record. Our data contribute to the debate on modern human dispersal patterns by providing age estimations for UP assemblages containing modern human fossils. Comparison of our age estimations with those of European AMH fossils place Eltheruda's layer before the first occurrence of modern humans in Europe. Similarly, Egbert's layer predates any known Aurignacian and other early UP modern humans in Europe. The antecedence of both UP lithic technocomplexes and modern human remains in the Levant, the latter also corroborated by Manot 1, indicates that modern humans carrying a UP toolkit were present in the Levant before arriving in Europe. This contradicts Douka et al.'s (24) hypothesis that shell beads, and by proxy UP modern humans, appeared first in Europe. Observed similarities in early UP lithic technology and other material culture of Levantine and European technocomplexes suggest a close interrelation that could well result from dispersal events. In turn, this implies that the Levant served as a corridor for modern humans dispersing out of Africa and into Europe rather than being a "cul-de-sac" where modern humans arrived after they dispersed into Europe.

That the first occurrence of the Levantine IUP and Bohunician takes place in a short time window suggests rapid dispersal events over large geographical areas (17), and the same is true for the first occurrence of the Proto-Aurignacian (13). The spread of modern humans and their material culture has implications for the replacement of Neanderthals by modern humans and acculturation debates, because current data suggest that at the time of these dispersals the former were still present in some parts of Europe (57–59). Changes in material culture of some of the last Neanderthals in Europe could therefore be related to contact and subsequent (stimulus) diffusion of modern human behaviors.

Materials and Methods

All analyses (AMS radiocarbon dating, AAR, and oxygen isotopes) have been conducted in conjunction on selected specimens to enable direct comparison and contextualization of the results of various datasets (*SI Appendix*, Section 2). We selected samples based on an evaluation of the shell preservation by using both macroscopic attributes and physicochemical characteristics (XRD, staining with Feigl and Mutvei solutions) (*SI Appendix*, Section 2). Radiocarbon dating at the Groningen radiocarbon laboratory consists of chemical cleaning of the outer surface using a 4% (wt/vol) HCl solution, followed by CO_2 development using concentrated H_3PO_4. All dates were calibrated using the Marine13 (34) calibration curve and the software OxCal 4.2.4 (37). Reservoir correction (R) was carried out taking into account a local ΔR of 53 ± 43 B.P. for the eastern Mediterranean (60). AAR was used as a test for diagenetic integrity after Demarchi et al. (61). Sampling for oxygen isotope analysis was adopted after Mannino et al. (62). Grossman and Ku's (63) equation with a correction for the conversion of VSMOW to VPDB (64) was used to calculate SST from $\delta^{18}O_{shell}$ values. Mean $\delta^{18}O_{water}$ is based on pore water estimations (65) and corrected for MIS 3 glacial conditions. For a full description of our sampling and analysis methods, see *SI Appendix*, Section 2.

ANTHROPOLOGY

1. Klein RG (2008) Out of Africa and the evolution of human behavior. *Evol Anthropol* 17(6):267–281.
2. Trinkaus E, et al. (2003) An early modern human from the Peştera cu Oase, Romania. *Proc Natl Acad Sci USA* 100(20):11231–11236.
3. Mellars P (2006) Archeology and the dispersal of modern humans in Europe: Deconstructing the "Aurignacian." *Evol Anthropol* 15(5):167–182.
4. Forster P (2004) Ice Ages and the mitochondrial DNA chronology of human dispersals: A review. *Philos Trans R Soc Lond B Biol Sci* 359(1422):255–264.
5. Stringer C (2002) Modern human origins: Progress and prospects. *Philos Trans R Soc Lond B Biol Sci* 357(1420):563–579.
6. Hublin J-J (2014) The modern human colonization of western Eurasia: When and where? *Quat Sci Rev*, 10.1016/j.quascirev.2014.08.011.
7. Ewing JF (1960) Human types and prehistoric cultures at Ksar'Akil. Lebanon. Men and Cultures: Selected Papers Fifth International Congress Anthropological Ethnological Science Philadelphia. 1956:535–539.
8. Hershkovitz I, et al. (2015) Levantine cranium from Manot Cave (Israel) foreshadows the first European modern humans. *Nature* 520:216–219.
9. Kuhn SL, et al. (2009) The early Upper Paleolithic occupations at Uçağizli Cave (Hatay, Turkey). *J Hum Evol* 56(2):87–113.
10. Benazzi S, et al. (2011) Early dispersal of modern humans in Europe and implications for Neanderthal behaviour. *Nature* 479(7374):525–528.
11. Sinitsyn AA (2003) The most ancient sites of Kostenki in the context of the Initial Upper Paleolithic of northern Eurasia. *The Chronology of the Aurignacian and of the Transitional Technocomplexes: Dating, Stratigraphies, Cultural Implications*, eds Zilhao J, d'Errico F (Instituto Português de Arqueologia, Lisboa), pp 89–107.
12. Hoffecker JF, et al. (2008) From the Bay of Naples to the River Don: The Campanian Ignimbrite eruption and the Middle to Upper Paleolithic transition in Eastern Europe. *J Hum Evol* 55(5):858–870.
13. Davies W (2001) A very model of a modern human industry: New perspectives on the origins and spread of the Aurignacian in Europe. *Proc Prehist Soc* 67:195–217.
14. Tostevin GB (2012) *Seeing Lithics: A Middle-Range Theory for Testing for Cultural Transmission in the Pleistocene* (Oxbow Books, Oxford).
15. Svoboda JA, Bar-Yosef O (2003) *Stránská skála. Origins of the Upper Paleolithic in the Brno Basin, Moravia, Czech Republic* (Peabody Museum of Archaeology and Ethnology, Harvard University, Cambridge, MA).
16. Tsanova T (2013) The beginning of the Upper Paleolithic in the Iranian Zagros. A taphonomic approach and techno-economic comparison of Early Baradostian assemblages from Warwasi and Yafteh (Iran). *J Hum Evol* 65(1):39–64.
17. Bar-Yosef O (2007) The dispersal of modern humans in Eurasia: A cultural interpretation. *Rethinking the Human Revolution: New Behavioural and Biological Perspectives on the Origin and Dispersal of Modern Humans*, eds Mellars P, Boyle K, Bar-Yosef O, Stringer C (McDonald Institute for Archaeological Research, University of Cambridge, Cambridge, U.K.), pp 207–217.
18. Goring-Morris NA, Belfer-Cohen A (2003) *More Than Meets the Eye: Studies on Upper Palaeolithic Diversity in the Near East* (Oxbow Books, Oxford).
19. Bar-Yosef O (2002) The Upper Paleolithic revolution. *Annu Rev Anthropol* 31:363–393.
20. Gunz P, et al. (2009) Early modern human diversity suggests subdivided population structure and a complex out-of-Africa scenario. *Proc Natl Acad Sci USA* 106(15):6094–6098.
21. Hoffecker JF (2009) Out of Africa: Modern human origins special feature: The spread of modern humans in Europe. *Proc Natl Acad Sci USA* 106(38):16040–16045.
22. Fu Q, et al. (2014) Genome sequence of a 45,000-year-old modern human from western Siberia. *Nature* 514(7523):445–449.
23. Douka K (2013) Exploring the great wilderness of prehistory: The chronology of the Middle to the Upper Paleolithic transition in the northern Levant. *Mitteilungen der Gesellschaft Urgeschichte* 22:11–40.
24. Douka K, Bergman CA, Hedges REM, Wesselingh FP, Higham TF (2013) Chronology of Ksar Akil (Lebanon) and implications for the colonization of Europe by anatomically modern humans. *PLoS ONE* 8(9):e72931.
25. Ewing FJ (1947) Preliminary note on the excavations at the Palaeolithic site of Ksâr 'Akil, Republic of Lebanon. *Antiquity* 21(84):186–196.
26. Mellars P, Tixier J (1989) Radiocarbon-accelerator dating of Ksar 'Aqil (Lebanon) and the chronology of the Upper Palaeolithic sequence in the Middle East. *Antiquity* 63:761–768.
27. Azoury I (1986) *Ksar Akil, Lebanon: A Technological and Typological Analysis of the Transitional and Early Upper Palaeolithic Levels of Ksar Akil and Abu Halka* (BAR, Oxford).
28. Metni MC (1999) A re-examination of a proposed Neandertal maxilla from Ksar 'Akil rock shelter, Antelias, Lebanon. *Am J Phys Anthropol* S28:202.
29. Bergman CA (1988) Ksar Akil and the Upper Palaeolithic of the Levant. *Paléorient* 14(2):201–210.
30. van Regteren Altena CO (1962) Molluscs and echinoderms from Palaeolithic deposits in the rock shelter of Ksâr'Akil, Lebanon. *Zool Meded* 38(5):87–99.
31. Kuhn SL, Stiner MC, Reese DS, Güleç E (2001) Ornaments of the earliest Upper Paleolithic: New insights from the Levant. *Proc Natl Acad Sci USA* 98(13):7641–7646.
32. Douka K (2011) An Upper Palaeolithic shell scraper from Ksar Akil (Lebanon). *J Archaeol Sci* 38(2):429–437.
33. Dean JS (1978) Independent dating in archaeological analysis. *Adv Archaeol Method and Theory* 1:223–255.
34. Reimer PJ, et al. (2013) IntCal13 and Marine13 radiocarbon age calibration curves 0–50,000 years cal BP. *Radiocarbon* 55(4):1869–1887.
35. van der Plicht J (2012) Borderline radiocarbon. *Neth J Geosci* 91(1–2):257–261.
36. Higham T, et al. (2009) Problems with radiocarbon dating the Middle to Upper Palaeolithic transition in Italy. *Quat Sci Rev* 28(13–14):1257–1267.
37. Bronk Ramsey C (2009) Bayesian analysis of radiocarbon dates. *Radiocarbon* 51(1):337–360.
38. Sánchez Goñi M, et al. (2002) Synchroneity between marine and terrestrial responses to millennial scale climatic variability during the last glacial period in the Mediterranean region. *Clim Dyn* 19(1):95–105.
39. Svensson A, et al. (2008) A 60 000 year Greenland stratigraphic ice core chronology. *Climate of the Past* 4(1):47–57.
40. Vogel JC, Waterbolk HT (1963) Groningen radiocarbon dates IV. *Radiocarbon* 5:163–202.
41. Douka K, Hedges RM, Higham TG (2010) Improved AMS ^{14}C dating of shell carbonates using high-precision X-ray diffraction and a novel density separation protocol (CarDS). *Radiocarbon* 52(2):735–751.
42. Marks AE (1983) The Middle to Upper Paleolithic transition in the Levant. *Advances in World Archaeology* 2:123–136.
43. Shea JJ (2003) The Middle Paleolithic of the east Mediterranean Levant. *J World Prehist* 17(4):313–394.
44. Rebollo NR, et al. (2011) New radiocarbon dating of the transition from the Middle to the Upper Paleolithic in Kebara Cave, Israel. *J Archaeol Sci* 38(9):2424–2433.
45. Bar-Yosef O, et al. (1996) The dating of the Upper Paleolithic layers in Kebara cave, Mt Carmel. *J Archaeol Sci* 23(2):297–306.
46. Barzilai O, Alex B, Boaretto E, Hershkovitz I, Marder O (2014) The Early Upper Palaeolithic at Manot Cave, Western Galilee, Israel. *PESHE* 3:34.
47. Marom A, McCullagh JSO, Higham TFG, Sinitsyn AA, Hedges REM (2012) Single amino acid radiocarbon dating of Upper Paleolithic modern humans. *Proc Natl Acad Sci USA* 109(18):6878–6881.
48. Haesaerts P, Damblon F, Sinitsyn A, van der Plicht J (2004) Kostienki 14 (Voronezh, Central Russia): New data on stratigraphy and radiocarbon chronology. Section 6: Le Paleolithique superieur / The Upper Palaeolithic: Sessions generals et posters / General sessions and posters, Acts of the XIVth UISPP Congress, University of Liege, Belgium, 2–8 September 2001, eds Dewez M, Noiret P, Teheux E (BAR Int Ser 1240), pp 169–180.
49. Kuhn SL, Zwyns N (2014) Rethinking the initial Upper Paleolithic. *Quat Int* 347:29–38.
50. Zilhão J (2006) Neandertals and moderns mixed, and it matters. *Evol Anthropol* 15(5):183–195.
51. Le Brun-Ricalens F, Bordes J-G, Eizenberg L (2009) A crossed-glance between southern European and Middle-Near Eastern early Upper Palaeolithic lithic technocomplexes. existing models, new perspectives. *The Mediterranean from 50 000 to 25 000 BP: Turning Points and New Directions*, eds Camps M, Szmidt C (Oxbow Books, Oxford), pp 11–33.
52. Richter D, Tostevin G, Skrdla P, Davies W (2009) New radiometric ages for the Early Upper Palaeolithic type locality of Brno-Bohunice (Czech Republic): Comparison of OSL, IRSL, TL and ^{14}C dating results. *J Archaeol Sci* 36(3):708–720.
53. Nigst PR (2012) *The Early Upper Palaeolithic of the Middle Danube Region* (Leiden University Press, Leiden).
54. Szmidt CC, Normand C, Burr GS, Hodgins GW, LaMotta S (2010) AMS ^{14}C dating the Protoaurignacian/Early Aurignacian of Isturitz, France. Implications for Neanderthal-modern human interaction and the timing of technical and cultural innovations in Europe. *J Archaeol Sci* 37(4):758–768.
55. Douka K, Grimaldi S, Boschian G, del Lucchese A, Higham TF (2012) A new chronostratigraphic framework for the Upper Palaeolithic of Riparo Mochi (Italy). *J Hum Evol* 62(2):286–299.
56. Schmidt C, et al. (2013) First chronometric dates (TL and OSL) for the Aurignacian open-air site of Românești-Dumbrăviţa I, Romania. *J Archaeol Sci* 40(10):3740–3753.
57. Semal P, et al. (2009) New data on the late Neandertals: Direct dating of the Belgian Spy fossils. *Am J Phys Anthropol* 138(4):421–428.
58. Hublin J-J, et al. (2012) Radiocarbon dates from the Grotte du Renne and Saint-Césaire support a Neandertal origin for the Châtelperronian. *Proc Natl Acad Sci USA* 109(46):18743–18748.
59. Higham T, et al. (2014) The timing and spatiotemporal patterning of Neanderthal disappearance. *Nature* 512(7514):306–309.
60. Reimer PJ, McCormac FG (2002) Marine radiocarbon reservoir corrections for the Mediterranean and Aegean Seas. *Radiocarbon* 44(1):159–166.
61. Demarchi B, et al. (2013) Intra-crystalline protein diagenesis (IcPD) in *Patella vulgata*. Part I: Isolation and testing of the closed system. *Quat Geochronol* 16(100):144–157.
62. Mannino MA, Thomas KD, Leng MJ, Sloane HJ (2008) Shell growth and oxygen isotopes in the topshell *Osilinus turbinatus*: Resolving past inshore sea surface temperatures. *Geo-Mar Lett* 28(5–6):309–325.
63. Grossman EL, Ku T-L (1986) Oxygen and carbon isotope fractionation in biogenic aragonite: Temperature effects. *Chem Geol Isot Geosci Sect* 59:59–74.
64. Dettman DL, Reische AK, Lohmann KC (1999) Controls on the stable isotope composition of seasonal growth bands in aragonitic fresh-water bivalves (Unionidae). *Geochim Cosmochim Acta* 63(7):1049–1057.
65. Paul HA, Bernasconi SM, Schmid DW, McKenzie JA (2001) Oxygen isotopic composition of the Mediterranean Sea since the Last Glacial Maximum: Constraints from pore water analyses. *Earth Planet Sci Lett* 192(1):1–14.

Supporting Information

New chronology for Ksâr 'Akil (Lebanon) supports Levantine route of modern human dispersal into Europe

Marjolein D. Bosch, Marcello A. Mannino, Amy L. Prendergast, Tamsin C. O'Connell, Beatrice Demarchi, Sheila Taylor, Laura B. Niven, Johannes van der Plicht, and Jean-Jacques Hublin

Section 1: Ksâr 'Akil

Site background

Location

Ksâr 'Akil (KSA), which translates to "inaccessible or high place", rockshelter is situated in the Antelias Valley (1–3), roughly 10 km northeast of Beirut (Lebanon). The valley is named after the town where the valley terminates in the Bay of St. George. About 2 km inland from this bay, the valley previously split into two smaller ones, which surrounded a limestone hill with a Semitic "high place" on top (1), probably lending its name to the rockshelter. This hill has been quarried away almost to the valley bottom (4). The Ksâr 'Akil rockshelter itself, located on the northern slope of the valley, still survives, albeit filled with rubble from the quarrying activities (4).

In prehistoric times, the south-facing opening of the rockshelter would have been protected by the hill in the center of the valley. Fresh water supply would likely have come from the adjacent Antelias River running down the valley. Furthermore, the Ksâr 'Akil occupants would have had access to the small coastal plain (sahil), the steep slopes of the Lebanon Mountains, and the open highlands of the El Beqaa Valley (Fig. S1.1).
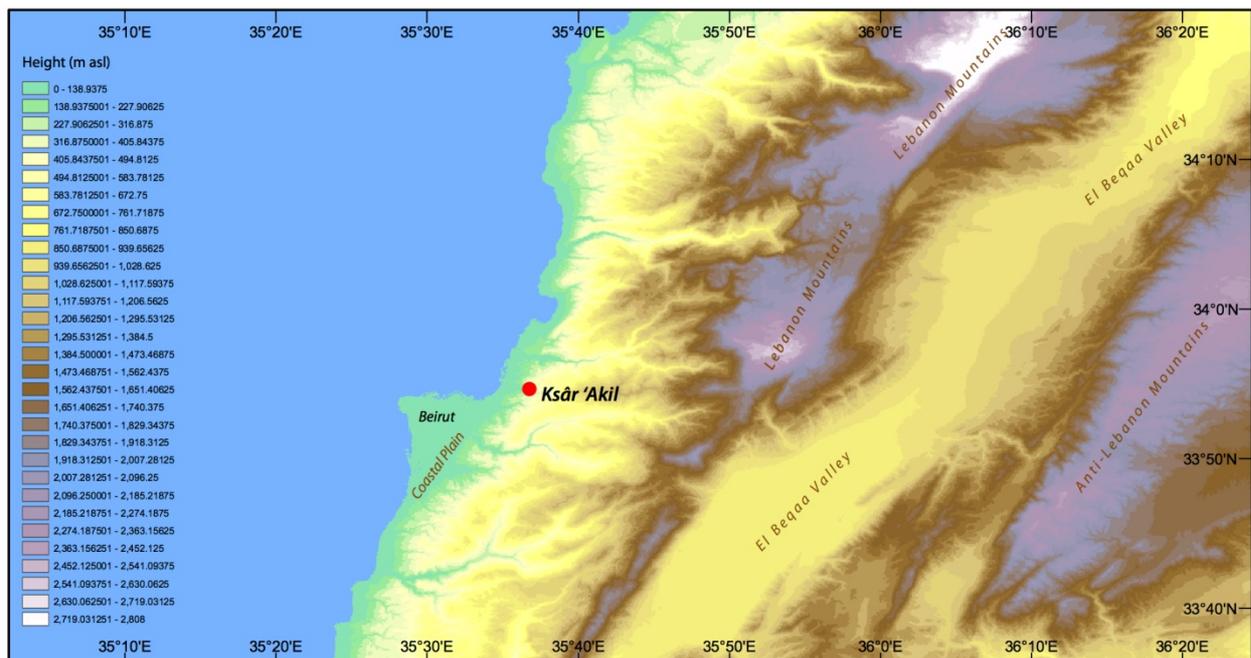
Figure S1.1. Geographical location of Ksâr 'Akil, Lebanon. Digital elevation data based on NASA's Shuttle Radar Topography Mission (SRTM) (downloaded from: https://lta.cr.usgs.gov/SRTM).

History

The site was discovered in 1922 when a treasure hunter bought Ksâr 'Akil and started digging its deposits for gold (5). Professor E. Day, a geologist at the University of Beirut, learned of this activity and acquired some of the uncovered lithics and faunal material. The lithics were subsequently sent to Paris and London for identification where, among others, Abbé H. Breuil had the opportunity to study the materials. It was on his recommendation that a team led by Rev. J. G. Doherty from Boston

College go to Lebanon to conduct the first scientific excavations at the site in 1937 (1). In the first two seasons (1937 and 1938), deposits were excavated up to a depth of 19 m. After a break forced by World War II, Doherty and Ewing led the last excavation season (1947–1948) when bedrock was eventually reached at 23 m below datum (5). In 1969, J. Tixier reopened the site and continued excavations until 1975, reaching a depth of 9 m, when his team was forced to leave Lebanon due the outbreak of civil war (6, 7).

The 23-m sequence of Ksâr ʻAkil contains deeply-stratified deposits, spanning the Middle Paleolithic (MP) to the Epipaleolithic (EPI) (Fig. S1.2). The lowermost 7 m (16–23 m below datum) contain alluvial deposits with evidence of MP occupation (3, 5). During this period of deposition, Ksâr ʻAkil was likely occasionally flooded by the nearby stream depositing reddish alluvial sediments (3). Above 16 m, the sediments containing Upper Paleolithic (UP) artifacts are generally brown-greyish in color and intersected by complexes (e.g., at 16–17 m and 10–11 m) of red clay bands underlying a deposit of angular limestone blocks. Wright (3) suggests that the red clay, at least for the band at 10–11 m, is the result of *in situ* pedogenesis stemming from either an episode of non-habitation or a period of intensified weathering due to increased rainfall. Both Wright (3, 8) and Ewing (9) hypothesized that periods of clay formation coincided with humid climatic conditions, potentially representing pluvial sub-phases of the last glaciation.

The material under study here comes from the 1930s and 1940s excavations by Doherty, the only one to reach the Initial Upper Paleolithic (IUP) and Early Upper Paleolithic (EUP) layers. Although excavation techniques were not up to present-day standards, all sediments were dry sieved and special care was taken when excavating animal bones in anatomical association (10). Ewing (1, 2, 9) was responsible for curating the faunal (and human) remains in the field from 1938 onwards and made a preliminary, very detailed, and impressively accurate account of faunal distribution throughout the sequence. The envisioned fully-blown paleontological study was originally delegated to D. Bate, a specialist of Pleistocene Near Eastern faunas at the Natural History Museum in London, UK. However, she was not able to complete her study before her death in 1951. Therefore, the Ksâr ʻAkil fauna was subsequently sent to D. Hooijer at the Natural History Museum in Leiden, the Netherlands, who carried out a study of all vertebrates (11). During his investigations, Hooijer separated the vertebrates and invertebrates, and the latter were given to his colleague C. O. van Regteren-Altena for study (12). A. Kersten kindly provided us with lists based on notes from the original excavators that correlate depths per square to the layers assigned by Ewing and thus linking the material from the 1937-8 and 1947-8 excavations. Both faunal assemblages from Ksâr ʻAkil remain stored in the Naturalis Biodiversity Center in Leiden.
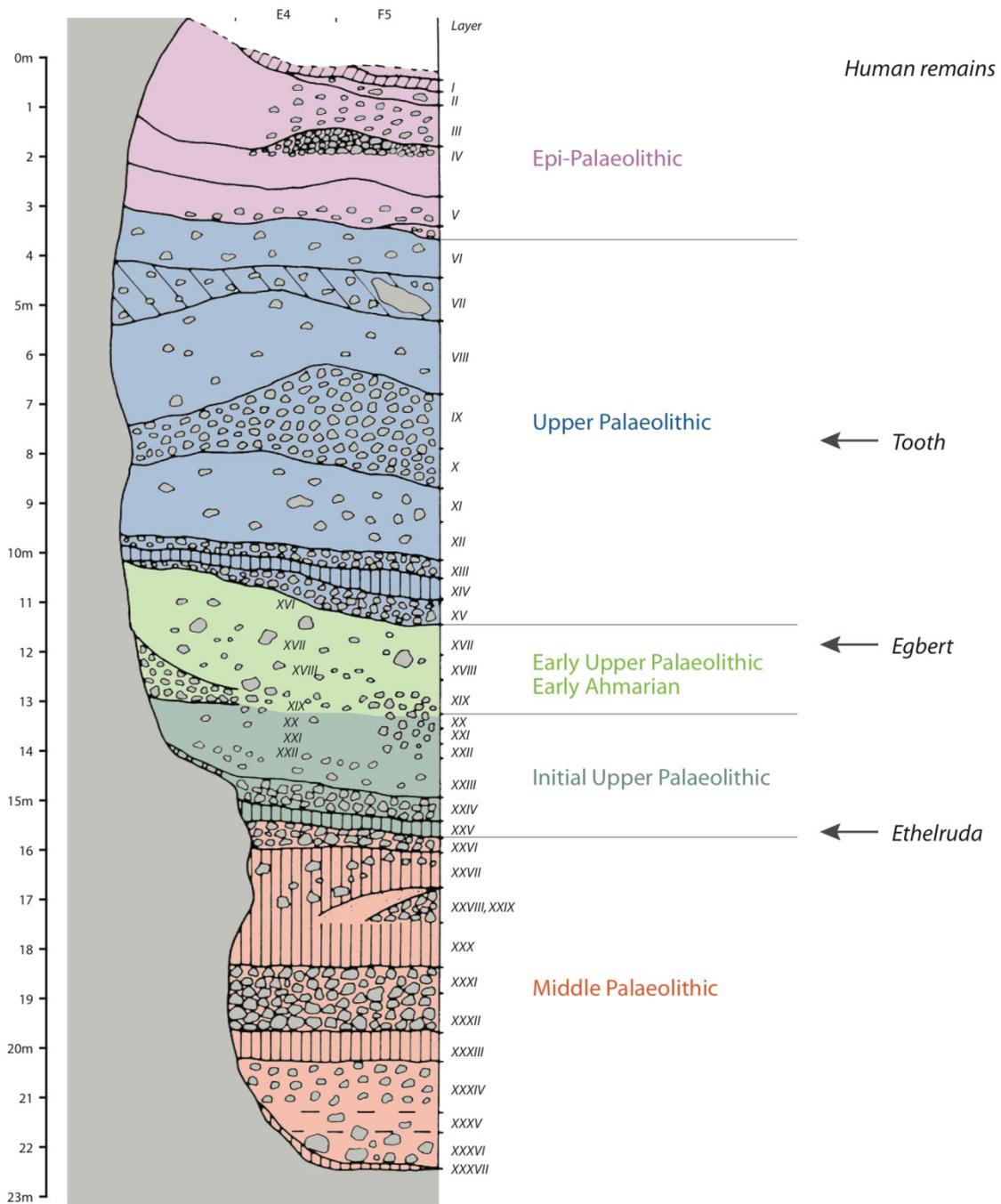
Figure S1.2. Ksâr 'Akil stratigraphic sequence (redrawn after (6) with reference to the major archeological divisions and human remains).

Over time, scholars have divided the Ksâr 'Akil sequence in several phases based either on changes in lithic technology (6, 13–15) or differences in faunal composition (11). In general, these divisions follow the same succession for the UP, i.e., from IUP/Emirian/transitional via EUP/Early Ahmarian and UP/Levantine Aurignacian to Epipaleolithic/proto-Kebaran deposits, although analogous packages are often labeled differently and individual layers are sometimes placed in different archeological phases (Table S1.1). Changes in faunal composition coincide with some, but not all, such boundaries. In this study, we generally follow the most recent division by Williams and Bergman (14), with the exception of grouping all named and unnamed UP assemblages into one UP (6). We have also sought to refer to individual layers so that the conclusions of our work may also be used within the frameworks proposed by other scholars.

Table S1.1. Division of the Upper Paleolithic sequence of Ksâr 'Akil phases based on lithic typology (6, 14, 15) and changes in faunal composition (11). Abbreviations: EPI: Epipaleolithic, UP: Upper Paleolithic, EUP: Early Upper Paleolithic, IUP: Initial Upper Paleolithic, Aur: Aurignacian.

Layer	Mellars & Tixier	Kuhn et al.	Williams & Bergman	Hooijer
I	EPI	early Kebaran	EPI (phase 7)	phase 6
II				
III				
IV				
V				
VI	UP	late Levantine Aur	Atlian (phase 6)	phase 5
VII			Levantine Aur (phase 5)	
VIII				
IX			Unnamed UP (phase 4)	phase 4
X				
XI		mid Levantine Aur	Unnamed UP (phase 3)	
XII		early Levantine Aur		
XIII				
XIV	Transitional phase B	UP II B	Ahmarian (phase 2)	
XV				
XVI				
XVII				
XVIII				
XIX		UP II A		phase 3
XX				
XXI	Transitional phase A	UP I	IUP (phase 1)	
XXII				
XXIII				
XXIV				
XXV				

Fauna

The IUP and EUP deposits at Ksâr 'Akil provided the bulk of both vertebrate and invertebrate faunal remains. In the framework of the doctoral research of the principle author, all invertebrate and

vertebrate material of several selected IUP and EUP layers were subjected to a detailed zooarcheological study. The analysis of the UP vertebrates is still ongoing. Preliminary zooarcheological investigations indicate that the vertebrate remains are heavily fragmented (84%), albeit in reasonable condition (Fig. S1.3a). Bone weathering is commonly low (Fig. S1.3b), given that most specimens can be assigned to weathering stages 1–2 after Behrensmeyer (16). The bones were subjected to a mild form of acid treatment (soaked in 10% acetic acid solution overnight) to dissolve adhering sediment, after which any remaining reaction was stopped by a base-wash (10% sodium carbonate solution). After acid treatment, the cortical surface preservation is generally >50% (Fig. S1.3c). The majority of bones are not burned, but all burning stages, both carbonized (stages 1–3) and calcined (stages 4–6), after Stiner et al. (17), are present (Fig. S1.3d). Carnivore modifications are extremely rare (Fig. S1.4a) and human modifications in the form of cutmarks and impact fractures occur in about 11% of the assemblage (Fig. S1.4b).
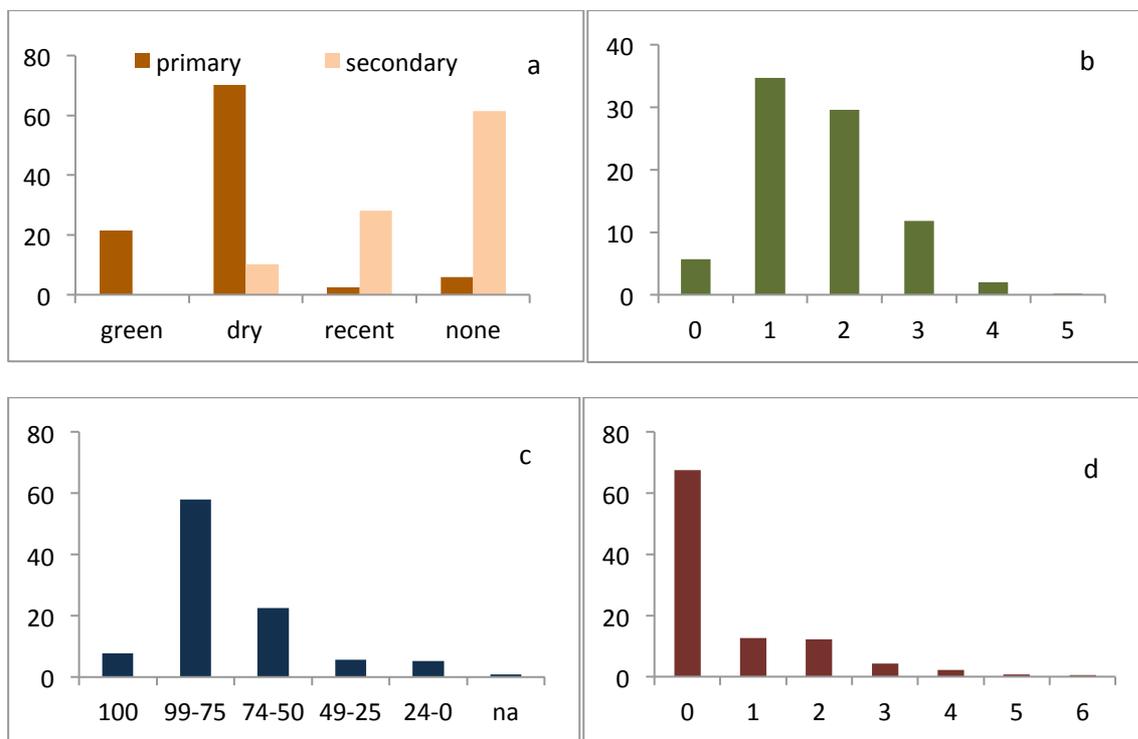
Figure S1.3. Bone preservation in the Upper Paleolithic at Ksâr 'Akil. Percentage NISP of a) Primary and secondary bone breakage, b) Bone weathering stages after Behrensmeyer (16), c) Cortical bone preservation, and d) Bone burning stages after Stiner et al. (17).

6

a

modification type	n	%
toothmark	7	0.13
puncture	2	0.04
gnawing	1	0.02
none	5250	99.81

b

modification type	n	%
cutmark	347	6.59
impact	251	4.76
chopmark	1	0.02
none	4670	88.63
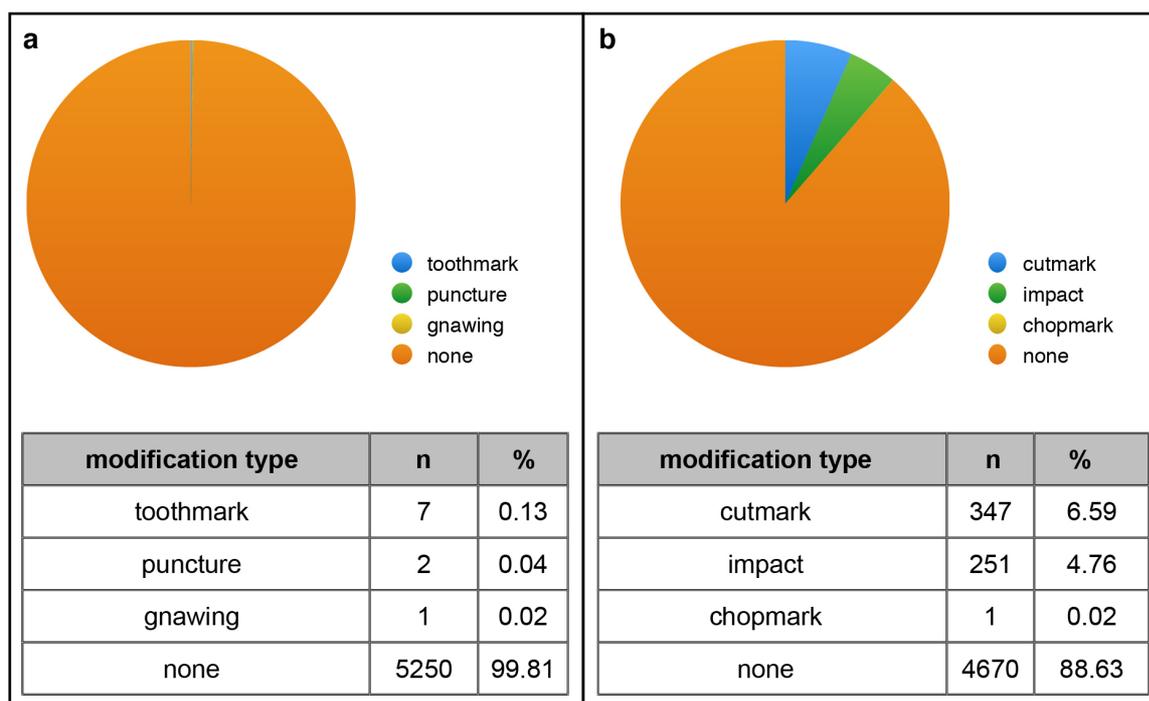
Figure S1.4. Bone modifications in the Upper Paleolithic at Ksâr 'Akil. NISP and percentage NISP of a) carnivore modifications and b) human modifications.

IUP faunal exploitation

IUP Layers XXV and XXII were selected for detailed vertebrate faunal analysis. Preliminary investigations identified the following taxa: aurochs, ibex, wild goat, gazelle, red deer, Mesopotamic fallow deer, roe deer, wild boar, spur-thighed tortoise, hare, birds, and several carnivores (Fig. S1.5). During the IUP, faunal exploitation mainly took place in wooded areas, probably on the seaward slopes of the Lebanon Mountains, and partly on the coastal plain. The low frequency of open habitat arid species suggests that the highlands of the Beqaa Valley were less often targeted or that portions of hunted animals were not taken back to the site (Fig. S1.6). The main prey species include Mesopotamic fallow deer in combination with wild goat, wild boar, and aurochs (Fig. S1.5). Marine resources were exploited for consumption in low quantities, although empty shells were often collected to be used as tools or ornaments.

EUP faunal exploitation

Zooarcheological investigations were conducted for EUP Layers XVIII, XVI, and XIV. In our preliminary study, the same taxa were identified as those recovered in the IUP (Fig. S1.5). During the EUP or Early Ahmarian, the majority of terrestrial faunal remains are of woodland species, suggesting that hunting primarily took place in surrounding forested hills (Fig. S1.6). Small-bodied open habitat and arid species, such as gazelles, were exploited slightly more often than in the IUP. Overall, EUP faunal exploitation was more evenly distributed, i.e., taxa were hunted in more similar frequencies, than in the IUP. Mesopotamic fallow deer was still the dominant species, although red deer, aurochs, ibex, wild goat, gazelle, wild boar, and spur-thighed tortoise increased (Fig. S1.5). Among the invertebrate remains, edible species (i.e., intertidal gastropods) gained in importance relative to "non-food" species.
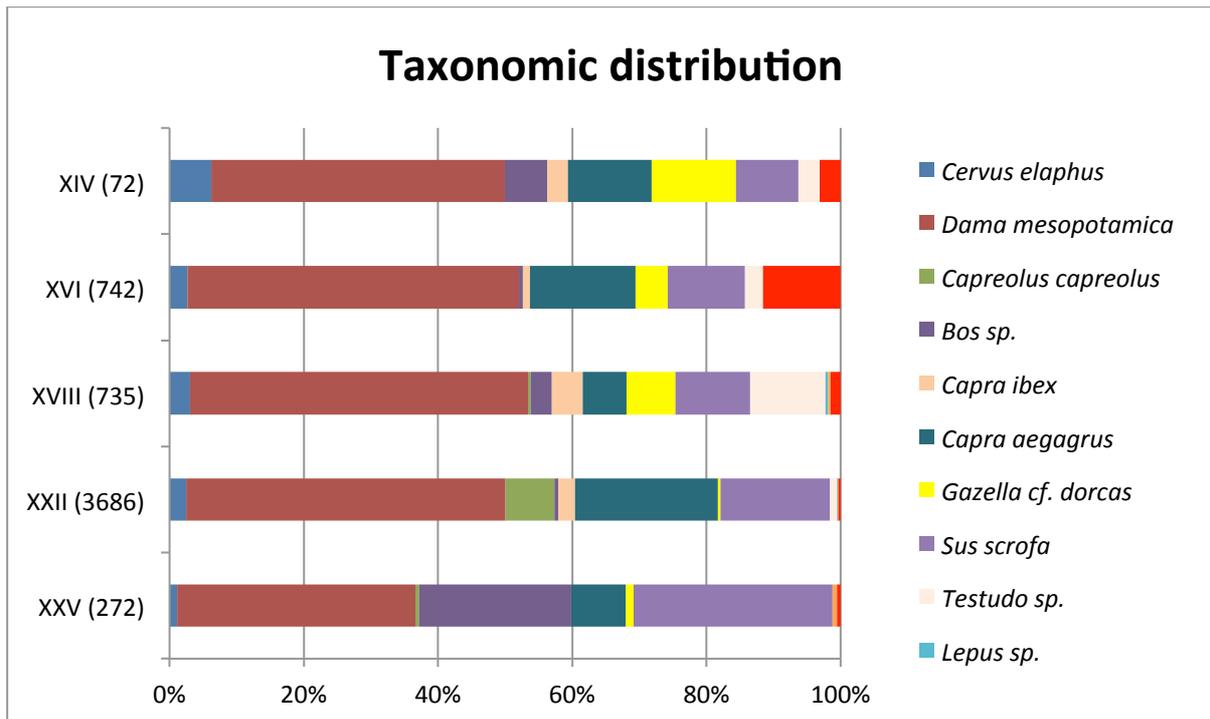
Figure S1.5. Taxonomic distribution. Percentages of exploited vertebrate faunal remains per studied layer (number of remains). Percentages are based on the number of identifiable specimens (NISP) per layer.
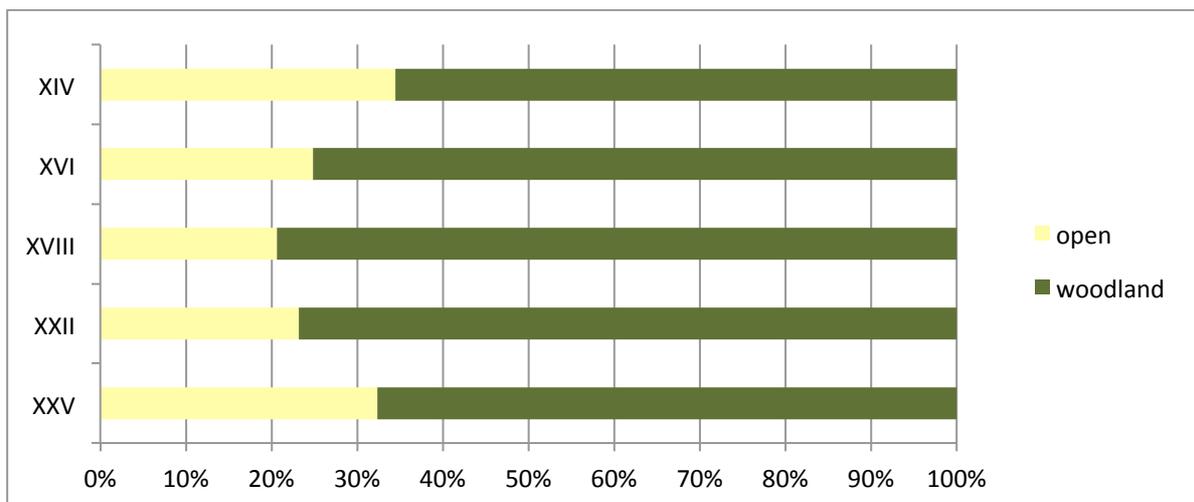
Figure S1.6. Frequency of habitat types of exploited terrestrial taxa. The frequency is based on the number of identifiable specimens (NISP) per layer. Division of woodland versus open/arid species is after Shea (18).

Invertebrate fauna

The invertebrate faunal assemblage studied here consists of 3571 specimens (n). The number of specimens that could be identified to species or family level (NISP) and for which a secure stratigraphic position could be ascertained on the basis of their labels is 3406 (see Table S1.2). We undertook a detailed archeomalacological study of the assemblage. Mollusks from Ksâr 'Akil include terrestrial, freshwater, and marine species. Most mollusk remains are from EUP and later UP deposits. Small amounts of mollusks were found in the Epipaleolithic layers and only a single specimen was found in the Middle Paleolithic deposits.

Table S1.2. Ksâr 'Akil mollusks. Number of identified specimens (NISP) per layer.

Species	I	II	III	IV	V	VI	VII	VIII	IX	X	XI	XII	XIII	XIV	XV	XVI	XVII	XVIII	XIX	XX	XXI	XXII	XXIII	XXIV	XXVIIIA
marine gastropods																									
Patella caerulea		1			1	2	21	6	2	1	1					1	4								
Patella rustica	1	1	1		18	7	6	1	3	3						9	19								
Patella ulyssiponensis						2	2	2								1	1								
Patella sp.				1	1	2	7	1	3		1						11	2		1					
Trochidae											1						1								
Phorcus articulatus									1		8						2								
Phorcus turbinatus			14	5	120	25	34	13	19	21	43	7	7			37	71	6	7	2		1			
Phorcus sp.									3		60	3					10		1						
Bolma rugosa											3												2		
Cerithium vulgatum							1		2		1					10	5		4	5	4	13	2		
Naticarius hebraeus																		1				1			
Neverita josephinia											1						2		1			1			
Semicassis saburon		1																							
Euthria cornea																1	2								
Pisania striata									1		1														
Columbella rustica					3	2	20	16	132	37	5	4		1	1	31	115	4	10	4	2	19	2	1	
Tarantinaea lignarius																	2								
Nassarius gibbosulus				1	7	9	31	59	145	26	8	10	1			37	125	14	25	10	26	128	10	1	
Nassarius mutabilis									1																
Nassarius sp.																				1		1			
Bolinus brandaris																	2								
Hexaplex trunculus							2		2							2	5								
Murex sp.									1											1					
Mitra cornicula									1							1									
Conus ventricosus						3			4	1							5	2		3					
marine gastropod									2	13							5			2		1			
marine bivalves																									
Acanthocardia tuberculata		1						4	14	1	2					7	31	2				2	1		
Acanthocardia sp.								1			2														
Cerastoderma glaucum																	1								
Donax trunculus									1																
cf. *Callista chione*																	1	1							
Venus verrucosa																	1								
Anadara cf. *polii*									2																
Arca noae																	1								
Barbatia barbata																		1							
Glycymeris nummaria					1				2			1				10	7		1			1		1	
Glycymeris sp.		1		3	1		2	5	26	1	9	1			1	34	78	16	29	7	23	22	6	6	
Lima lima									4								2								
Ostrea edulis									1												1		1		2
Spondylus gaederopus											1	1											1		
Pinna nobilis				1					3																
marine scaphopods																									
Antalis dentalis									10																
Antalis vulgaris									13	1															
Antalis sp.								2	13																
freshwater gastropods																									
Theodoxus jordani									4										1						
Melanopsis praemorsa						1			2										1						
freshwater bivalves																									
Unionacea						1		2	1																
Potomida littoralis									1																

9

Table S1.2. continued

Species	I	II	III	IV	V	VI	VII	VIII	IX	X	XI	XII	XIII	XIV	XV	XVI	XVII	XVIII	XIX	XX	XXI	XXII	XXIII	XXIV	XXVIIIA
terrestrial gastropods																									
Pomatias elegans																	1		1						
Pomatias olivieri					2	1	7	7	6	4	1	2	2			10	10	13	6	1		1			
Buliminus labrosus							2	1			1							2							
Pene syriacus								1											1						
Cristataria porrecta											1														
Oxychilus syriacus					3	1	1	4		2							2	1	1						
Helicidae											69						3		5	5					
Helix engadensis	1	1	13	12	80	42	125	64	21	9	21	4	1	2		16	44	2	8		2				
Sphincterochila cariosa					1																				
Metafructicola berytensis					2	5	5	4	2	3						13	12	4	10	1		2			
Monacha nummus																		1			1				
Monacha syriaca					2	3	4	1	7	1							6		4			2			
terrestrial gastropod										2	211	16					46		62	2					
total NISP	2	6	28	22	242	103	273	195	446	119	465	51	11	3	2	220	633	72	177	46	60	197	22	9	2

Taphonomic investigations reveal marked differences between marine species from different habitats (Table S1.3). Rocky shore intertidal gastropods were generally not exposed to marine taphonomic processes and were likely live-collected. Other marine gastropods, bivalves, and scaphopods show heavy marine alterations in the form of beach-wear and bioerosion and were collected empty probably from active or fossil beach deposits. The collection of empty shells took place for various purposes, for instance to use them as tools (19) or body ornaments (15, 20). Intertidal rocky shore gastropods were likely exploited for subsistence purposes. Human collection of these species is evident from edge damage on *Patella* spp. This is consistent with damage resulting from prying the limpets off the rocks. Other human modifications include the removal of the apex of *Phorcus* spp., probably to facilitate flesh extraction (Fig. S1.7). This evidence, together with the fact that they were collected live, strongly suggests that these species were used as food. Occasional burning (n=667) resulting in a combination of heat cracks, discoloration, and decalcification was observed in the assemblage. This burning damage might either result from indirect (while buried) or direct (while on the surface) exposure to heat. Indirect exposure to heat might have occurred by lighting a fire on top of deposits containing shell and, therefore, was not necessarily deliberate (17).

Patella rustica　　*Phorcus turbinatus*
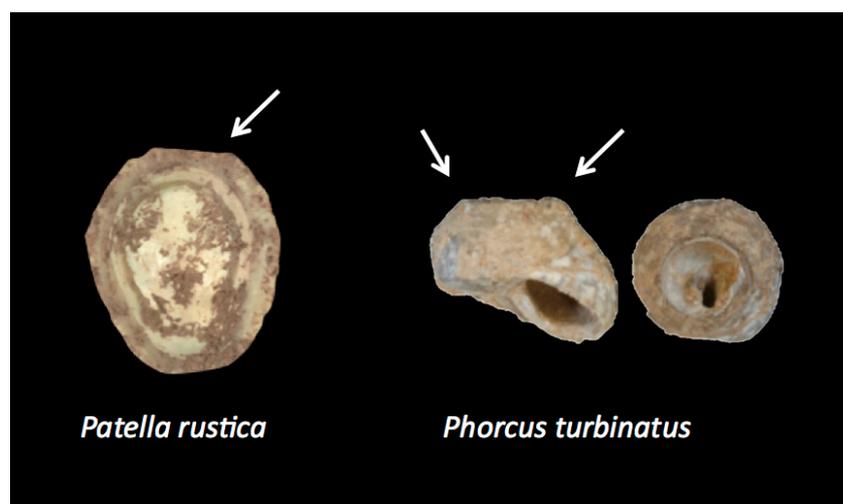
Figure S1.7. Examples (marked by arrows) of human modifications on intertidal rocky shore gastropods. Edge damage on *Patella rustica* (left) congruent with damage resulting from forcing live specimens loose from the rocks they live on and the removal of the apex of *Phorcus turbinatus* (right) to aid flesh extraction.

Table S1.3. Marine taphonomic alterations. n: number; %: percentage relative to the total marine mollusk assemblage. "Food:" numbers of marine alterations for species collected for consumption (i.e., rocky shore intertidal gastropods: *Phorcus turbinatus, Phorcus articulatis, Patella rustica, Patella caerulea* and *Patella ulyssiponensis)*; "Non-food:" numbers of marine alterations for marine mollusk species transported to the site for purposes other than consumption (e.g., used as tools and ornaments). Note: shells may show more than one type of taphonomic alteration. Therefore, the total number of marine taphonomic altered shells (last row) is less than the sum of all individual marine taphonomic alterations.

Marine taphonomic alterations	n	%	Food	Non-food
Bioerosion	38	1.59	0	38
epizootic encrustation	4	0.17	0	4
reducing atmosphere	36	1.51	0	36
beach washed	867	36.38	1	866
gastropod damage	50	2.10	0	50
crab damage	72	3.02	1	71
boring sponge damage	263	11.04	0	263
total marine alterations	**989**	**41.50**	**2**	**987**

Section 2: Geochemical methods

Introduction

We applied an array of zooarcheological, geochronological, and geochemical techniques on the shells of the rocky shore intertidal gastropod *P. turbinatus*. By dating a species of shellfish gathered for consumption, the objective of this study was to reconstruct when UP humans were present at the site and exploiting marine resources. The species *P. turbinatus* was selected because it is the most abundant taxon exploited as food and, thus, representative of past environments and behaviors pertaining to the occupation of Ksâr 'Akil. Previous studies have shown that the oxygen isotope composition of *P. turbinatus* is an accurate record of sea surface temperature (SST) (21, 22) and that this species can be used to obtain reliable AMS radiocarbon dates (23, 24). AMS radiocarbon dating on *P. turbinatus* specimens has allowed us to refine the chronology of the site and episodes of mollusk collection. AAR analyses were used to provide an independent estimate of the diagenetic integrity of the intra-crystalline proteins trapped in the shells. Dated shells were also sampled for oxygen isotope analyses to reconstruct SSTs. Moreover, all analyses were conducted in conjunction on selected specimens (Fig. S2.1; Table S2.1) allowing correlation of the results from the different lines of investigation (25).

Sample selection

Zooarcheological and specifically taphonomic investigations have shown that intertidal rocky shore species collected for consumption were the best-preserved species in the assemblage (see SI section 1). Individual *P. turbinatus* specimens were selected for study based on their excellent preservation, as determined by a set of macroscopic and chemical characteristics. Shells were initially selected if they had visible mother-of-pearl layers (i.e., inside the aperture) and, preferentially, when these were translucent, as in living specimens. Care was also taken to avoid shells with ante mortem damage and visible growth-stops parallel to the aperture edge. *P. turbinatus* shells are bimineralic and consist of an aragonitic inner nacreous layer and an outer prismatic layer of calcite (23, 26). Diagenetic alterations are more easily detectable in the aragonitic part of the shell than the calcitic part because aragonite is a less stable crystal phase than calcite (26) (but see (27)). We conducted X-ray diffraction analysis of the inner nacreous layer to confirm that the aragonite was still pristine and had not recrystallized into calcite. A portion of the dated shells (n=5) was also sectioned along the periphery of the outer whorl (perpendicular to the axis of growth) with a Buehler Isomet 1000 precision saw, set in resin, ground, and polished to inspect microgrowth increments. These sections were initially stained with Mutvei solution (28), a blue substance that etches microgrowth-structures, allowing them to be examined. Intact microstructures suggest no recrystallization of carbonate occurred after death and, thereby, that the primary aragonitic structure of the shell is intact. The Mutvei solution was later removed by successively grinding with 400, 800, and 1200 µm powder and Feigl solution (see Fig. S2.5 D–E) applied to differentiate calcite from aragonite within the shell (29). Aragonite reacts faster to Feigl solution (after roughly 20 min) than calcite (after approximately a day) making it possible to detect diagenetic substitutions of primary aragonite with secondary calcite in the nacreous layer (30). Well-preserved *P. turbinatus* shells were then sampled

to obtain sequences of oxygen isotope values for SST reconstruction. The top part of the shell (i.e., the apex or directly below in instances where the apex had already been cut off by the Paleolithic inhabitants of Ksâr 'Akil) was mechanically cleaned of adhering sediment and sent to the Centre for Isotope Research of the University of Groningen for AMS radiocarbon dating. The basal part of the shell (including part of the lip) was sent to the NEaar laboratory of the University of York for amino acid racemization analyses.

Table S2.1. List of samples showing layer, square, and laboratory numbers for oxygen isotope analysis (Oxygen), amino acid racemization (NEaar) and AMS radiocarbon dating. RGM-nr: museum inventory number (Naturalis Biodiversity Center, Leiden). Note: all specimens of one species with identical provenience (i.e., layer, square, depth below datum) were combined and given a single RGM-number and, therefore, we have assigned a unique sample ID (KSA nr) to all specimens under study and refer to this number in the SI text. To ease interpretation, radiocarbon dated samples are referred to by only their layer or with a sub-number (e.g., XVI (1)) when more dates are available.

KSA nr (Oxygen)	RGM-nr	layer (ref in text)	Square	NEaar lab ID (AAR)	GrA nr (^{14}C)
KSASV04	606336	V	F3-6	8700	-
KSASV03	606336	V	F3-6	8701	-
KSASV02	606338	V	E4-6	8702	-
KSASV01	606338	V	E4-6	8703	-
KSAS01V	606338	V	E4-6	8704	53005
KSASVI04	606337	VI	E4,FG3-4	8695	-
KSASVI03	606337	VI	E4,FG3-4	8696	-
KSASVI02	606337	VI	E4,FG3-4	8697	-
KSASVI01	606337	VI	E4,FG3-4	8698	-
KSAS08VI	606337	VI	E4,FG3-4	8699	54848
KSASXI02	606317	XI	E5	8692	-
KSASXI01	606317	XI	E5	8693	-
KSAS02XI	606317	XI	E5	8694	53006
KSAS11XII	606921	XII	E4	9344, 9345	57545
KSAS07XVI	606334	XVI (1)	E5	8691	54847
KSAS10XVI	606310	XVI (2)	F3	9346, 9347	57544
KSASXVI02	606334	XVI (3)	E5	8689	57598
KSASXVI03	606334	XVI (4)	E5	8688	57599
KSASXVI04	606334	XVI	E5	8687	-
KSASXVI01	606334	XVI	E5	8690	-
KSAS03XVII	606306	XVII (1)	F4	8686	53001
KSAS06XVII	606306	XVII (2)	F4	8685	54846
KSASXVII01	606309	XVII (3)	E4	8684	57602
KSASXVII02	606309	XVII (4)	E4	8683	57603
KSASXVII03	606306	XVII	F4	8682	-
KSAS09XVIII	606308	XVIII	E4	9348, 9349	57542
KSAS04XIX	639387	XIX	F4	-	53004
KSAS12XX	606294	XX	F4	-	57597
KSAS05XXII	606420	XXII	F4	-	53000
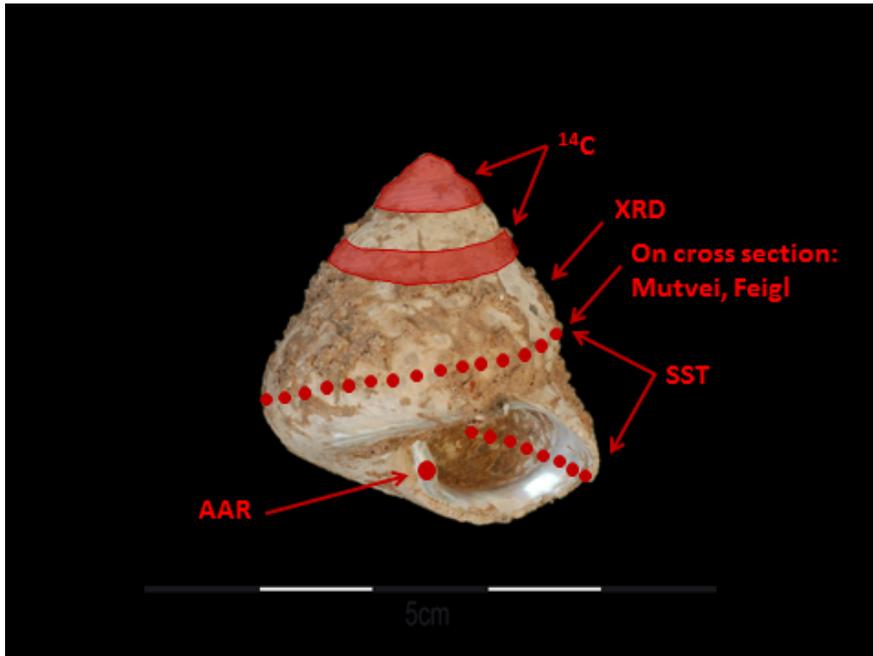
Figure S2.1. *Phorcus turbinatus* with sampling spots for the different analyses. [14]C: AMS radiocarbon dating, XRD: X-ray diffraction, Mutvei: Mutvei solution (28), Feigl: Feigl solution (29), SST: Sequences (all small red dots) of oxygen isotope samples for sea surface temperature reconstruction, AAR: amino acid racemization. Scale bar in cm.

Radiocarbon dating

Samples

We sampled 16 *Phorcus turbinatus* shells from the Upper Paleolithic part of the sequence for AMS radiocarbon dating (Table S2.2). The selected species allowed us to date the antiquity of shellfish exploitation and estimate the timing of IUP and EUP occupation at Ksâr 'Akil. Dating well-preserved specimens of a taxon collected for consumption allows us to attain accurate dates for human occupation linked to this behavior, because like other mollusks, *P. turbinatus* needs to be consumed fresh. Thus, its death coincides with the time of human collection, consumption, and discard.

Table S2.2. AMS radiocarbon samples. BP: uncalibrated radiocarbon years before present; +/-: Error at one sigma level; cal BP: calendar years before 1950. Calibration conducted using the Marine13 calibration curve (31) and OxCal 4.2.4 software (32). Dates were corrected for the global mean reservoir age (R: i.e., 400 years) with a local correction or ΔR of 53 ± 43 (33). Calibrated ages are shown at 68.2% and 95.4% probability.

KSA nr	Layer	Laboratory nr	Date BP	+/-	age cal BP (68.2%)	age cal BP (95.4%)
KSAS01V	V	GrA-53005	26,210	130/120	30,210–29,700	30,430–29,500
KSAS08VI	VI	GrA-54848	28,810	130/130	32,550–31,930	32,790–31,690
KSAS02XI	XI	GrA-53006	34,310	230/210	38,660–38,090	38,890–37,590
KSAS11XII	XII	GrA-57545	35,880	260/230	40,340–39,690	40,710–39,360
KSAS07XVI	XVI (1)	GrA-54847	39,910	370/320	43,470–42,850	43,930–42,620
KSAS10XVI	XVI (2)	GrA-57544	35,960	230/210	40,390–39,800	40,730–39,520
KSASXV102	XVI (3)	GrA-57598	37,320	270/240	41,730–41,230	41,950–40,930
KSASXV103	XVI (4)	GrA-57599	39,890	310/280	43,400–42,870	43,770–42,650
KSAS03XVII	XVII (1)	GrA-53001	34,090	220/200	38,460–37,770	38,640–37,200
KSAS06XVII	XVII (2)	GrA-54846	39,850	340/310	43,390–42,830	43,800–42,600
KSASXVII01	XVII (3)	GrA-57602	36,730	240/220	41,240–40,650	41,460–40,340
KSASXVII02	XVII (4)	GrA-57603	38,260	260/240	42,310–41,920	42,510–41,720
KSAS09XVIII	XVIII	GrA-57542	36,290	240/220	40,780–40,160	41,100–39,880
KSAS04XIX	XIX	GrA-53004	39,390	330/290	43,050–42,570	43,330–42,340
KSAS12XX	XX	GrA-57597	40,040	340/300	43,560–42,950	43,990–42,730
KSAS05XXII	XXII	GrA-53000	40,550	350/310	44,060–43,340	44,430–43,070

Dates

The 16 AMS radiocarbon dates were obtained from the Centre for Isotope Research of the University of Groningen (Table S2.2) and are consistent with the stratigraphic division. Our data show that the earliest shellfish exploitation in the IUP Layer XXII dates to 40,550 +350/-310 BP. The start of the Early Ahmarian (*sensu lato*; Layer XX) dates to 40,040 +340/-300 BP. A shell fragment from Layer XIX dates to 39,390 +330/-290 BP. There are nine dates for Layers XVIII–XVI considered by most scholars to belong to the "classic" Early Ahmarian (34) showing a wide range of age estimations from 39,910 +370/-320 to 34,090 +220/-200 BP. The dates of 36,290 +240/-220 BP obtained for Layer XVIII and 34,090 +220/-200 BP for layer XVII are unexpectedly young relative to other dates obtained from the same layer or subsequent, overlying layers. The Upper Paleolithic Layers XII, XI, and VI (also named Atlian) were dated to 35,880 +260/-230 BP, 34,310 +230/-210 BP, and 28,810 ± 130 BP, respectively. The start of the Epipaleolithic or Proto-Kebaran (Layer V) was dated to 26,210 +130/-120 BP. The latter two dates are slightly older than expected for Atlian and Proto-Kebaran lithic industries (35), but fit well with the dates on charcoal obtained by Mellars and Tixier (6) (Table S2.3).

Two conventional dates were obtained decades ago by Vogel and Waterbolk (36) on land snails (GrN-2195) and on charred material (GrN-2579). GrN-2195 was made on shells collected between 6 and 7.5 m below datum (Layers VII–IX). GrN-2579 with a date of 43,750 ± 1500 BP is probably a minimum age due to uncertainty as to the type of the dated material (i.e., charcoal as suggested by Wright (3) or a dark clay band containing organic material or charred bone (see (36)). It has erroneously been reported as Gro-2574-75 by Wright (3).This date has been variously placed in

Layer XXVI or XXVII (37, 38). However, based on the original descriptions of the stratigraphy as it was known at the time, it more likely comes from layer XXV or the boundary between XXV–XXVI. Vogel and Waterbolk (36) describe the provenience of the sample as "a dark clay band at 16 m level 1 m below the top of the Upper Levalloisian-Mousterian" and provide references (1) for further details. Wright (3) describes two red clay layers at 16 and 17 m below datum that are associated with (overlying) layers of angular stones, although in his stratigraphic drawing (3) they appear to be at 15 and 16 m depth. He further notes that the partly alluvial deposits stop at 16 m below datum (3). Ewing (1) describes the same two angular stone/clay complexes (Complex 3 and 4), but places them at 15 and 16 m depth. Complex 3 is made up of a layer of angular stones (XXIV) and a layer of red clay (XXV). Complex 4 is composed in a similar way (i.e., Layer XXVI angular stones and layer XXVII red clay). In Ewing's (5) drawing of the stratigraphy, a depth of 16 m coincides with the boundary between stone complexes 3 and 4, which is 1 m below the start of the Upper Levalloiso-Mousterian layers. It also coincides with a significant faunal change including the disappearance of rhinoceros (which we ascertained can be placed in Layer XXV; see SI section 1). Thus, sample GrN-2579 probably comes from the boundary between Layers XXVI and XXV, perhaps more likely from the upper Layer XXV, as both Wright (3) and Vogel and Waterbolk (36) describe it originating from a clay substrate. Considered a minimum age, the date corresponds well with our minimum age estimation for Layer XXV, where the human fossil of Ethelruda was found (Tables S2.3, S2.5).

Table S2.3. List of all previous radiocarbon dates for Ksâr 'Akil. Layers after Ewing (5); dates in uncalibrated radiocarbon years. Note: the two dates in pink are the same date, but reported differently by different scholars.

Layer	Laboratory nr.	Date	+/-	Sample material	Reference
III	MC-410	24,400	900	Land snail	(38)
III	OxA-1791	23,170	400	Charcoal	(6)
III	OxA-1792	22,850	400	Charcoal	(6)
III	OxA-1793	22,020	360	Charcoal	(6)
III	OxA-1794	22,480	380	Charcoal	(6)
III	OxA-1795	22,850	380	Charcoal	(6)
V–VI	MC-1191	26,500	900	Charcoal	(6)
V–VI	OxA-1796	21,100	500	Charcoal	(6)
V–VI	OxA-1797	26,900	600	Charcoal	(6)
V–VI	OxA-1798	29,300	800	Charcoal	(6)
VII	OxA-1803	30,250	850	Charcoal	(6)
VII	OxA-19194	30,250	170	Charcoal	(37)
VIII	OxA-20875	30,640	160	*Nassarius gibbosulus*	(37)
VII–IX	GrN-2195	28,840	380	Shell	(36)
IX	OxA-1804	31,200	1300	Charcoal	(6)
IX	OxA-1805	32,400	1100	Charcoal	(6)
IX	OxA-20022	37,210	230	*Glycymeris* sp.	(37)
IX	OxA-20023	30,360	140	*Nassarius gibbosulus*	(37)
X	MC-1192	32,000	1500	Charcoal	(6)
X	OxA-25585	34,550	250	*Nassarius gibbosulus*	(37)

Table S2.3. Continued

| Layer	Laboratory nr.	Date	+/-	Sample material	Reference
XII	OxA-20024	35,520	200	*Nassarius gibbosulus*	(37)
XV	OxA-20876	35,020	240	*Nassarius gibbosulus*	(37)
XVI	OxA-22665	36,040	240	*Nassarius gibbosulus*	(37)
XVII	OxA-X-2342-57	28,130	110	*Columbella rustica*	(37)
XVII	OxA-20877	36,270	240	*Glycymeris* sp.	(37)
XVII	OxA-22269	35,390	250	*Acanthocardia* sp.	(37)
XVII	OxA-20487	33,930	220	*Nassarius gibbosulus*	(37)
XVII	OxA-25652	33,300	230	*Columbella rustica*	(37)
XVII	OxA-20486	35,780	240	*Nassarius gibbosulus*	(37)
XVIII	OxA-X-2338-8	33,760	210	*Columbella rustica*	(37)
XVIII	OxA-25653	34,830	240	*Nassarius gibbosulus*	(37)
XVIII	OxA-20488	34,230	210	*Nassarius gibbosulus*	(37)
XIX	OxA-22664	35,510	240	*Nassarius gibbosulus*	(37)
XIX	OxA-X-2361-14	32,960	160	*Columbella rustica*	(37)
XX	OxA-20879	35,010	240	*Nassarius gibbosulus*	(37)
XXI	OxA-20025	36,390	210	*Nassarius gibbosulus*	(37)
XXII	OxA-25655	30,890	160	*Columbella rustica*	(37)
XXII	OxA-20880	34,940	200	*Nassarius gibbosulus*	(37)
XXII	OxA-22667	34,320	190	*Nassarius gibbosulus*	(37)
XXIII	OxA-20489	36,790	270	*Nassarius gibbosulus*	(39)
XXIII	OxA-20490	37,430	320	*Nassarius gibbosulus*	(39)
16 m	Gro-2574-75	44,400		Charcoal	(3)
XXV/(XXVI)	GrN-2579	43,750	1500	dark clay band	(36)
XXVIII	OxA-X-2361-17	33,810	180	*Ostrea* sp.	(37)
XXVIII	OxA-X-2361-23	35,900	400	*Ostrea* sp.	(37)
XXVIII	OxA-20491	39,310	330	*Ostrea* sp.	(37)
XXVIII A	OxA-25656	39,530	330	*Ostrea* sp.	(37)
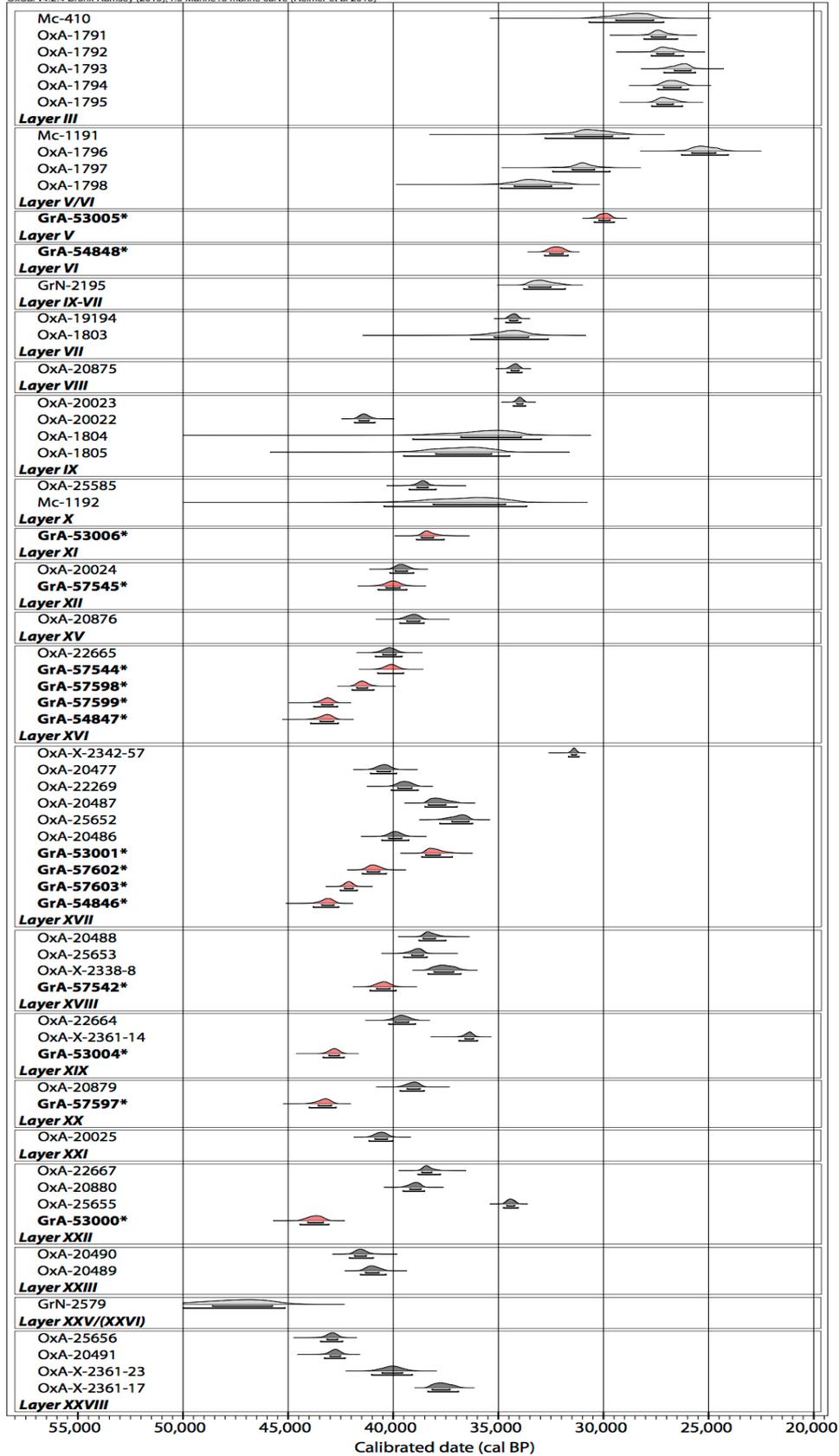
Figure S2.2. All age estimations for Ksâr 'Akil calibrated with OxCal 4.2.4 (32), dates of terrestrial samples with IntCal13 and those of marine samples with Marine13 calibration curve (31) using a

delta R of 53 ± 43 for the eastern Mediterranean (33). Light grey: dates by Mellars & Tixier (6) and Vogel & Waterbolk (36); Dark grey: dates by Douka et al. (37, 39); Red: dates reported in this paper. Note: For date GrN-2195 on land snails of unknown species it was impossible to calculate an accurate reservoir effect and was calibrated with IntCal13 (100% atmospheric). It is displayed only for completeness, but the calibrated age should be treated with caution.

Bayesian modeling

Calibration and Bayesian modeling of the AMS radiocarbon dates on *P. turbinatus* shell carbonates was conducted using the Marine13 calibration curve (31) and the OxCal 4.2.4 software package (32). Our samples were corrected for reservoir age, which is the offset between the atmospheric and the ocean carbon ratio that results of the upwelling of old carbon from deep oceanic water. The pre-industrial global mean reservoir correction (R) is about 400 years. Additionally, local fluctuations in upwelling intensity (ΔR) are used to fine-tune marine calibration corrections. We used a ΔR value of 53 ± 43 as an estimation for the Eastern Mediterranean by Reimer & McCormac (33).

Several Bayesian models were constructed using prior information regarding the provenience of the samples within the general stratigraphy. In the first model, all samples of a layer were placed in a phase. Boundaries were inserted at points where changes in lithic technology were observed (6, 14), allowing for the potential time elapsed between these technologically distinct periods. In general, the OxCal agreement index (A_model) of the resulting model should have a similar value as the agreement indices of individual measurements and should in any case not be below 60% (31). An outlier analysis was carried out as described by Bronk Ramsey (40). Initially, all measurements were given a prior outlier probability of 0.05. In subsequent steps, dates that were in poor agreement with the model resulting from the previous step were given increasingly higher prior outlier probabilities until the resulting Bayesian model and individual measurements had acceptable agreement indices (i.e., A_model and A_ind >60). The resulting model (hereafter model 1) has an agreement index A_model of 118.2% and has identified samples XVI (2–3), XVII (1, 3–4) and XVIII as outliers (see main text Fig. 1 for the model; Fig. S2.3 for the model configuration; Table S2.4 for the outliers; Table S2.5 for the calibrated and modeled age ranges). To test the robustness of our model we ran several variants of the outlier analysis (i.e., varying the prior outlier probabilities) all resulting in similar outcomes. In an alternative model, we considered that the young age of sample XVIII might indicate a gap in time between layers XIX and XVIII and separated the EUP in two phases. Kuhn et al. (14) identified a change in lithic technology (see Table S1.1) at this point in the sequence, between what they call UPII A (Layers XX-XIX) and UPII B (XVIII-XIV). Similarly, Hoojier (11) described a shift in fauna, between his Phase 3 (Layers XXV-XIX) and phase 4 (Layers XVIII-X). The resulting model (hereafter model 2; Fig. S2.4; Table S2.6) has the same amount of outliers (i.e., 6 namely samples: XVI (1, 3–4), XVII (1–2, and 4)) as model 1, but it shows a lower overall agreement index (A_model) of 83.5%. The main difference between these two models is the duration of the EUP (or UP IIA-B) and the modeled age for layer XVII, in which Egbert was found. The implications of these differences and a more detailed evaluation of models 1 and 2 are discussed below.

```
Plot()
{
 Outlier_Model("General",T(5),U(0,4),"t");
 Sequence()
 {
  Curve("Marine13","Marine13.14c");
  Delta_R("LocalMarine",53,43);
  Date("Ethelruda");
  Boundary("start dated IUP");
  Phase("Layer XXII")
  {
   R_Date("GrA-53000", 40550, 350);
   {
    Outlier(0.05);
   };
  };
  Boundary("end dated IUP");
  Boundary("start Ahmarian");
  Phase("Layer XX")
  {
   R_Date("GrA-57597", 40040, 340);
   {
    Outlier(0.05);
   };
  };
  Phase("Layer XIX")
  {
   R_Date("GrA-53004", 39390, 330);
   {
    Outlier(0.05);
   };
  };
  Phase("Layer XVIII")
  {
   R_Date("GrA-57542", 36290, 240);
   {
    Outlier(1.00);
   };
  };
  Phase("Layer XVII")
  {
   R_Date("GrA-54846", 39850, 340);
   {
    Outlier(0.05);
   };
   R_Date("GrA-57603", 38260, 260);
   {
    Outlier(0.50);
   };
   R_Date("GrA-57602", 36730, 240);
   {
    Outlier(0.50);
   };
   R_Date("GrA-53001", 34090, 220);
   {
    Outlier(1.00);
   };
   Date("Egbert");
  };
  Phase("Layer XVI")
  {
   R_Date("GrA-54847", 39910, 370);
```

```
 {
  Outlier(0.20);
 };
 R_Date("GrA-57599", 39890, 310);
 {
  Outlier(0.20);
 };
 R_Date("GrA-57598", 37320, 270);
 {
  Outlier(0.50);
 };
 R_Date("GrA-57544", 35960, 230);
 {
  Outlier(0.50);
 };
};
 Boundary("end Ahmarian");
 Boundary("start UP");
 Phase("Layer XII")
 {
  R_Date("GrA-57545", 35880, 260);
  {
   Outlier(0.05);
  };
 };
 Phase("Layer XI")
 {
  R_Date("GrA-53006", 34310, 230);
  {
   Outlier(0.05);
  };
 };
 Phase("Layer VI")
 {
  R_Date("GrA-54848", 28810, 130);
  {
   Outlier(0.05);
  };
 };
 Boundary("end UP");
 Boundary("start EPI");
 Phase("Layer V")
 {
  R_Date("GrA-53005", 26210, 130);
  {
   Outlier(0.05);
  };
 };
 Boundary("end EPI");
 };
};
```

Figure S2.3. Configuration (CQL code) of the Bayesian model presented in the main text (model 1).

Table S2.4. Prior and Posterior Outlier Probabilities results (model 1).

Element	Prior Outlier Probability	Posterior Outlier Probability	Model	Type
GrA-53000; 40550, 350	5	2	General	T
GrA-57597; 40040, 340	5	1	General	T
GrA-53004; 39390, 330	5	1	General	T
GrA-57542; 36290, 240	100	100	General	T
GrA-54846; 39850, 340	5	1	General	T
GrA-57603; 38260, 260	50	96	General	T
GrA-57602; 36730, 240	50	100	General	T
GrA-53001; 34090, 220	100	100	General	T
GrA-54847; 39910, 370	20	9	General	T
GrA-57599; 39890, 310	20	9	General	T
GrA-57598; 37320, 270	50	96	General	T
GrA-57544; 35960, 230	50	100	General	T
GrA-53006; 34310, 230	5	3	General	T
GrA-53006; 34310, 230	5	3	General	T
GrA-54848; 28810, 130	5	16	General	T
GrA-53005; 26210, 130	5	3	General	T

Table S2.5. Calibrated age ranges and results of age modeling for the Ksâr 'Akil sequence (model 1).

Indices A_{model}=118.2 $A_{overall}$=115.4	Unmodelled age range (cal BP) 68.2%		Unmodelled age range (cal BP) 95.4%		Modelled range (cal BP) 68.2%		Modelled range (cal BP) 95.4%		Individual Agree-ment	Conver gence
	from	To	From	to	from	to	from	to		
end EPI Boundary					**30236**	**28853**	**30521**	**26032**		**98.7**
GrA-53005; 26210, 130	30205	29697	30430	29495	30213	29688	30490	29455	101.9	99.8
Phase Layer V										
start EPI Boundary					**30944**	**29783**	**32361**	**29500**		**99.2**
end UP Boundary					**32392**	**30809**	**36634**	**29866**		**96.2**
GrA-54848; 28810, 130	32553	31933	32794	31690	32706	31936	38432	31557	88.4	96.7
Phase Layer VI										
GrA-53006; 34310, 230	38658	38090	38888	37587	38665	38069	38938	37488	102.3	99.6
Phase Layer XI										
GrA-57545; 35880, 260	40336	39690	40710	39363	40285	39626	40681	39234	101.9	99.7
Phase Layer XII										
start UP Boundary					**41865**	**39988**	**42862**	**39726**		**99.4**
end Ahmarian Boundary					**43092**	**42760**	**43318**	**41253**		**99.3**
GrA-57544; 35960, 230	40391	39802	40731	39519	43112	42816	43342	41611	99.3	99.7
GrA-57598; 37320, 270	41725	41231	41950	40931	43111	42815	43322	41467	100	99.6
GrA-57599; 39890, 310	43397	42871	43770	42654	43107	42821	43337	41672	117.4	99.7
GrA-54847; 39910, 370	43471	42846	43925	42615	43107	42821	43337	41677	121.5	99.7
Phase Layer XVI										
Egbert					43162	42896	43383	42658		99.7
GrA-53001; 34090, 220	38455	37770	38635	37202	43162	42896	43395	42642	103	99.7
GrA-57602; 36730, 240	41236	40650	41464	40338	43163	42896	43393	42641	99.9	99.7
GrA-57603; 38260, 260	42310	41916	42514	41716	43164	42895	43378	42143	99.7	99.5
GrA-54846; 39850, 340	43390	42829	43798	42601	43157	42900	43314	42731	130.4	99.5
Phase Layer XVII										
GrA-57542; 36290, 240	40782	40157	41095	39875	43205	42943	43359	42794	99.4	99.6
Phase Layer XVIII										
GrA-53004; 39390, 330	43049	42569	43325	42339	43221	42956	43374	42820	75.8	99.7
Phase Layer XIX										
GrA-57597; 40040, 340	43561	42949	43986	42728	43244	42969	43415	42841	125.6	99.9
Phase Layer XX										
start Ahmarian Boundary					**43270**	**42975**	**43467**	**42843**		**99.7**
end dated IUP Boundary					**43781**	**43177**	**44205**	**43003**		**99.9**
GrA-53000; 40550, 350	44056	43336	44426	43071	44075	43428	44444	43204	107.9	99.9
Phase Layer XXII										
start dated IUP Boundary					**44578**	**43477**	**46094**	**43195**		**99.4**
Ethelruda					49386	45866	49390	44289		99.6

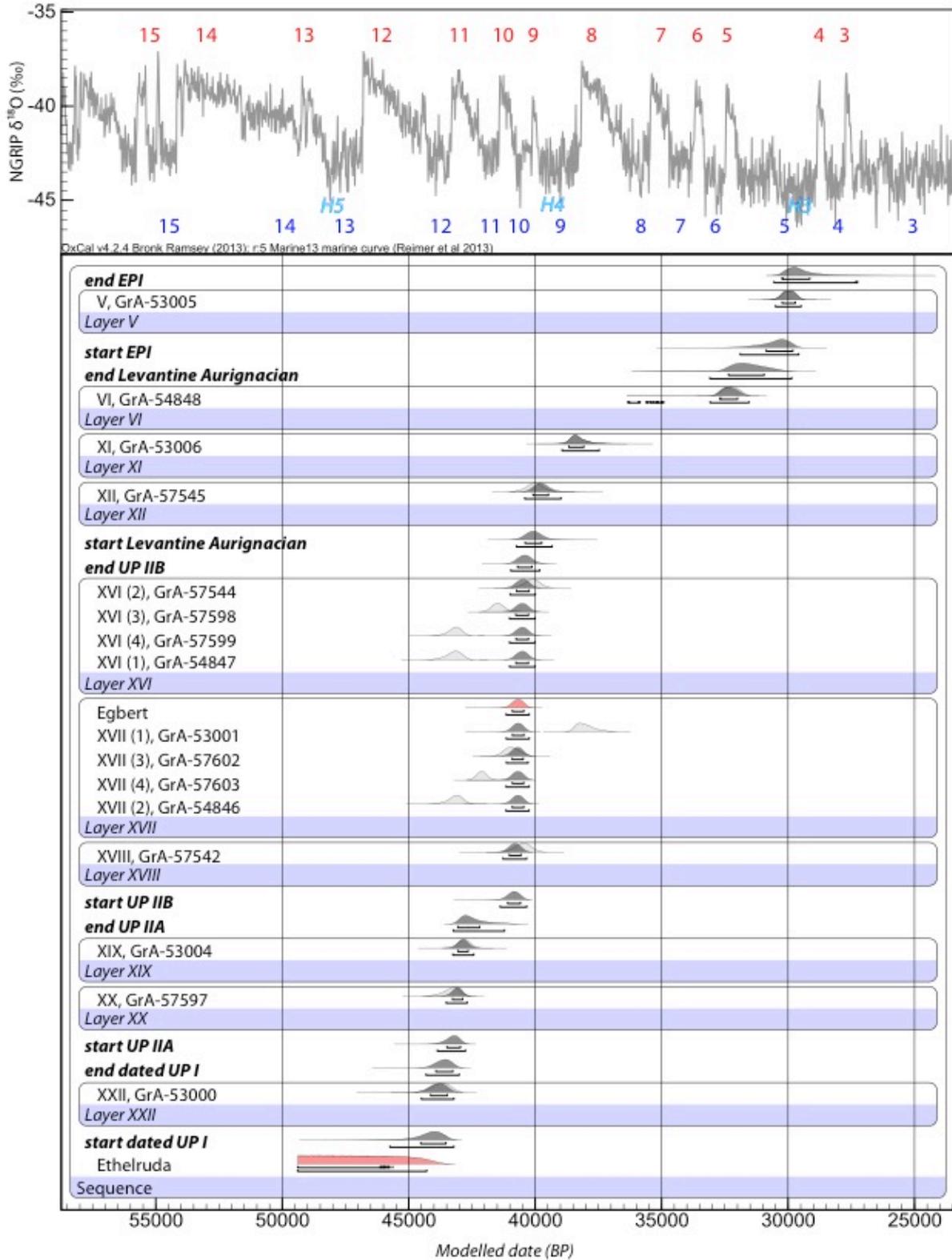Figure S2.4. Bayesian age model 2 for the Ksâr 'Akil sequence using OxCal 4.2.4 (32). The radiocarbon dates are calibrated using the Marine13 dataset (31) and ΔR value for the eastern Mediterranean (33). Light grey: individual radiocarbon likelihoods, dark grey: posterior probability distributions, red: PDFs for Ethelruda and Egbert's layers. The modeled data is compared with the NGRIP $\delta^{18}O$ curve

(grey), Greenland Interstadials (GIS; red) and Stadials (GS; blue) and Heinrich Events (H3-5; light blue).

Table S2.6. Calibrated age ranges and results of age modeling for the Ksâr 'Akil sequence (model 2).

Indices A_{model}=84.2 $A_{overall}$=88.1	Unmodelled age range (cal BP) 68.2%		Unmodelled age range (cal BP) 95.4%		Modelled range (cal BP) 68.2%		Modelled range (cal BP) 95.4%		Individual Agreement	Convergence
	from	To	From	to	from	to	from	to		
end EPI Boundary					**30232**	**29143**	**30557**	**27254**		**98.5**
GrA-53005; 26210, 130	30205	29697	30430	29495	30235	29714	30495	29485	101.9	99.8
Phase Layer V										
start EPI Boundary					**30867**	**29813**	**31890**	**29579**		**99.7**
end Levantine Aurignacian Boundary					**32355**	**30949**	**33093**	**29854**		**99.3**
GrA-54848; 28810, 130	32553	31933	32794	31690	32687	31997	36335	31550	95	99.1
Phase Layer VI										
GrA-53006; 34310, 230	38658	38090	38888	37587	38668	38075	38933	37468	101.6	99.6
Phase Layer XI										
GrA-57545; 35880, 260	40336	39690	40710	39363	40083	39475	40408	38979	89.8	99.7
Phase Layer XII										
start Levantine Aurignacian Boundary					**40397**	**39742**	**40743**	**39331**		**99.8**
end UP IIB Boundary					**40696**	**40127**	**40960**	**39822**		**99.5**
GrA-57544; 35960, 230	40391	39802	40731	39519	40737	40239	40986	39996	67.9	99.6
GrA-57598; 37320, 270	41725	41231	41950	40931	40764	40264	41015	40004	88.7	99.6
GrA-57599; 39890, 310	43397	42871	43770	42654	40757	40265	41012	40008	101.2	99.7
GrA-54847; 39910, 370	43471	42846	43925	42615	40761	40267	41012	40010	101.6	99.7
Phase Layer XVI										
<u>Egbert</u>					<u>40901</u>	<u>40449</u>	<u>41147</u>	<u>40237</u>		<u>99.7</u>
GrA-53001; 34090, 220	38455	37770	38635	37202	40898	40446	41140	40235	103.3	99.7
GrA-57602; 36730, 240	41236	40650	41464	40338	40910	40475	41135	40281	95.4	99.7
GrA-57603; 38260, 260	42310	41916	42514	41716	40904	40450	41149	40237	100.1	99.7
GrA-54846; 39850, 340	43390	42829	43798	42601	40905	40451	41154	40241	101.5	99.7
Phase Layer XVII										
GrA-57542; 36290, 240	40782	40157	41095	39875	41024	40559	41271	40338	82.4	99.7
Phase Layer XVIII										
start UP IIB Boundary					**41085**	**40583**	**41383**	**40334**		**99.1**
end UP IIA Boundary					**43056**	**42197**	**43231**	**41213**		**99.6**
GrA-53004; 39390, 330	43049	42569	43325	42339	43054	42649	43253	42428	112	99.9
Phase Layer XIX										
GrA-57597; 40040, 340	43561	42949	43986	42728	43266	42869	43515	42690	109.2	99.9
Phase Layer XX										
Start UP IIA Boundary					**43486**	**42955**	**43864**	**42756**		**99.9**
end dated UP I Boundary					**43923**	**43257**	**44312**	**43003**		**99.8**
GrA-53000; 40550, 350	44056	43336	44426	43071	44134	43478	44497	43213	105	99.8
Phase Layer XXII										
start dated UP I Boundary					**44520**	**43529**	**45741**	**43216**		**99.2**

Wide age ranges, as seen in Ksâr 'Akil Layers XVI and XVIII, are often encountered in organic samples dating to the Levantine IUP and EUP, even when up-to-date pre-treatment methods have been used (37, 41). This complicates the construction of chronologies for these types of sites, especially the ones like Ksâr 'Akil where the dated material comes from a museum collection rather than a freshly excavated sequence. This is evident from the high number of outliers in both considered Bayesian models (and also visible in the work of Douka et al. (37)). To determine which of the models is more accurate it is imperative to evaluate the integrity of individual dated samples. In general, the occurrence of outliers may result from 1) unsuccessful removal of contaminants in the sample, 2) post-depositional relocation (e.g., bioturbation), 3) burning, 4) excavation and/or curation errors, or 5) measurement errors. We have tried to avoid contamination by only using well-preserved and unburned specimens. We have also looked for potential markers of bioturbation or other forms of post-depositional, excavation, and curation errors like differential color and structure of adhering sediment in comparison to other specimens of the layer. Despite these efforts a small possibility always remains that intrusive material was wrongly included (e.g., perhaps sample XVII (1)). Wide age ranges might further be caused by (a) a long duration, of, e.g., the Early Ahmarian as suggested by model 2, (b) a disturbance of the later EUP (i.e., UP IIB; Layers XVIII-XIV) deposits by the occupants, or (c) an erosional event related to complex 2 (Layers XV-XIV; see SI section 1) resulting in extensive time-averaging of layer XVI specifically.

Regarding the age of the Early Ahmarian and its associated AMH fossil known as Egbert, our data suggest a time window of 43,400–37,800 cal BP or more likely 43,400–40,700 cal BP (excluding the XVII (1) date). The main difference between the two Bayesian models is the duration of the EUP (or UP IIA-B) between 43,300–43,100 cal BP (model 1) and between 43,500–40,100 cal BP (model 2), which also affects the estimated age for the Egbert fossil. Based on solely the output of the models it is hard to argue for/against either model. We therefore, investigated the integrity and taphonomic history of all individual samples through a study of intra-crystalline protein diagenesis and oxygen isotope analysis (see below).

Model 1 has a higher agreement index and is therefore probably more likely than model 2, but both models have the same number of outliers. While models are built on different prior information (e.g., different division in phases), both models consider samples XVII (1), XVII (4) and XVI (3) outliers. The age-estimation for the EUP in model 1 relies most on samples XX, XIX, XVII (2), XVI (1) and (4), whereas the UP IIB of model 2 draws heavily on samples XVIII, XVII (3), and XVI (2). Regarding sample XVIII, mean annual $\delta^{18}O_{shell}$ values (see below) indicate that the mollusk did not secrete its shell in the same temperature regime, and therefore did not live at the same time, as the other Ahmarian samples (with the exception of XVII (1), that is considered to be an outlier by both models). We therefore doubt that sample XVIII is indicative for the Ahmarian as a whole. As the corresponding AMS date is younger than most of the other Ahmarian samples coming from the layers above XVIII this date is more likely intrusive from higher up in the sequence rather than being residual from an older colder climatic phase. Further, sample XVII (3) does not fall entirely in the same diagenetic trajectory as the other samples (especially visible in the distribution of the amino-acid valine (THAA vs FAA; see discussion below and Fig. S2.6). This is an indication of open system behavior, and therefore the diagenetic integrity of this sample can be questioned.

We therefore argue that model 2, relying on two problematic dates (XVIII and XVII (3)), should be considered highly unlikely. This, in turn, implies that the Ahmarian at Ksâr 'Akil falls between 43,300 cal BP and 42,800 cal BP. The remains of Egbert are most likely from Layer XVII, as reported by the original excavator (1, 9). However, attempts to reconstruct Egbert's provenience from excavation notes and drawings have variously argued for an origin of the fossil from Layers XVI to XVIII (43), placing Egbert anywhere in these Early Ahmarian deposits. These uncertainties do not affect the modeled age for Egbert significantly due to the overall short time window modeled for the Early Ahmarian Layers XVI to XVIII in our model 1 (i.e., 43,200–42,800 cal BP).

During the Bayesian modeling, we used the "Date" function in OxCal to calculate probability distribution functions (PDF) for the age of the human fossils. In model 1, the date function provides a PDF of 43,200–42,900 cal BP (68.2% probability) for Egbert. Regarding the most likely age of Layer XXV's AMH human remains, known as Ethelruda, the lack of datable material from this layer and those directly above and below hampers precise age estimation. The date of the overlying IUP Layer XXII (i.e., > 44,100 cal BP) and the modeled start of the dated IUP (which has consistently been modeled to 44,600–43,500 cal BP in both models), nevertheless, provide *termini ante quem* for Ethelruda. The PDF for Ethelruda's layer provided by the "Date" function of OxCal extends beyond the end of the Marine13 calibration curve, but its upper limit of 45,900 cal BP provides a minimum age for the fossil. This minimum age fits well with the conventional radiocarbon date GrN-2579, probably from Layer XXV or the boundary of Layers XXV and XXVI (see discussion above).

Discussion of the dating approach in relation to other chronologies of Ksâr 'Akil

The largest discrepancies between our attempt to date the human occupation of Ksâr 'Akil and those of others occur in the lower part of the chronology and are provided by Douka et al. (38). They obtained AMS dates for 26 beach-collected shells of the taxa *Ostrea edulis, Glycymeris* sp., *Acanthocardia* sp., *Nassarius gibbosulus,* and *Columbella rustica.* They provided two Bayesian models, one similar to our approach assigning phases to individual layers (with 11 outliers) and one with the dates grouped per broader archeological phase (9 outliers). Similar to our set of radiocarbon dates, those of Douka et al. also have wide age ranges for the EUP/Ahmarian layers (36,000–28,000 BP) and for the IUP layers (i.e., 37,000–31,000 BP) (38). However, our age determinations are up to 4000 years older for the IUP and up to 3000 years older for the EUP (Fig. S2.2). These discrepancies in age estimations heavily influence any conclusions drawn regarding the start and duration of the IUP and EUP at Ksâr 'Akil, the first occurrence of modern humans in the Levant in relation to their first arrival in Europe, and the validity of the Levantine corridor hypothesis. The reasons behind the observed dissimilarity are currently unclear and further investigations are needed. The two studies used shells of different taxa that were used for different purposes by humans and that have different taphonomic histories. In addition, the samples were subjected to different pretreatment protocols and were dated in different radiocarbon laboratories. In the following text, we describe the potential effects of both approaches on the radiocarbon results in an effort to ascertain the causes of observed discrepancies.

Sample selection: Rationale

Our study selected *P. turbinatus,* which was gathered alive to be eaten by Paleolithic humans, while the species selected by Douka et al. (37) were collected empty from active or fossil beach deposits to be used as tools and ornaments. Exposure to different taphonomic environments could explain the observed divergence between our dates and those published by Douka et al. (37). Active beach

deposits are known for the temporal mixing or time-averaging effect they have on mollusk shell death assemblages (43–45). Shells might have undergone several burial and exhumation cycles in active beach deposits before they were picked up by humans. This process can continue for several thousands of years (44–46). Additionally, species that burrow in sandy substrates, like Glycymeridae, Acantocardidae, and Nassariidae, might be buried in sub-littoral sediments for periods of hundreds to thousands of years before they are washed ashore and are incorporated in active beach deposits (47). Therefore, individual shells from beached death assemblages or thanatocoenoses could have died thousands of years apart. These time-averaging processes would result in identical or older ages for beach-collected shells in relation to live-collected specimens and, although using beached specimens introduces a considerable uncertainty, this does not explain the inconsistency in age-estimations observed.

Post-mortem beach-collected shells would have additionally been exposed to a series of marine taphonomic processes, such as beach erosion or bioerosion (e.g., boring sponge damage). These taphonomic processes can heavily impact shell preservation and may have altered shell structure or made it more liable to post-depositional diagenesis. Abrasion and bioerosion result in pitting and fragmentation, which in turn enhance surface weathering (e.g., smoothing and decalcification). Decalcification is characteristic of shells subjected to diagenesis and also occurs in shells damaged by heat exposure. In the Ksâr 'Akil mollusk assemblage, decalcification that cannot be attributed to heating (i.e., no evidence of discoloration and/or heat cracks) is evident in 23.8% (n=355) of the beach collected species, but only in 0.2% (n=1) of *P. turbinatus* used in this study (Table S2.7). Therefore, *P. turbinatus* was likely less affected by diagenetic alterations than beach collected taxa.

Table S2.7. Decalcification observed macroscopically in species used for radiocarbon dating. Note: decalcification attributed to damage by heat exposure (i.e., that was accompanied by traces of discoloration, heat cracks and/or potlids) is excluded.

Species	NISP	n decalcified	% decalcified
Phorcus turbinatus	452	1	0.2
Acanthocardia tuberculata	66	7	10.6
Columbella rustica	429	80	18.7
Glycymeris sp.	299	99	33.1
Nassarius gibbosulus	696	169	24.3
total beach collected	1490	355	23.8

Post-mortem carbonate recrystallization is known to be the main cause for the introduction of younger carbon resulting in younger radiocarbon ages (39, 48, 49). Generally, this diagenesis results in the replacement of the more soluble aragonite by the more stable calcite. Busschers et al. (27) have demonstrated that, under saline conditions, microbial activity can also result in aragonite-to-aragonite substitutions. They further suggest that this phenomenon and the inherent introduction of young ^{14}C in the shells explain the recent (MIS 3) radiocarbon dates they obtained for Eemian (MIS 5e) North Sea mollusks. Eliminating contamination in shell carbonates is therefore problematic.

Ante-mortem incorporation of old carbon in shell carbonates is normally caused by mixing of sea surface waters with older oceanic carbon brought up by upwelling currents. The divergence between atmospheric and marine ^{14}C, known as reservoir effect (R), has been measured and modeled (50)

and can be corrected for. Local fluctuations in old carbon mixing occur and ΔR values for the Mediterranean Sea have been estimated to fine-tune the correction method (33, 51, 52). Hogg and Higham (53) have suggested that some intertidal marine species have enriched ^{14}C values compared to those of subtidal taxa. They argue that this is due to the intertidal species being exposed to the air (and atmospheric carbon) at low tides. If one corrects for a full marine environment in such cases, dates will be too young. However, shell growth does generally not occur when mollusks are out of the water (54). Minor growth lines that represent daily periods of non-growth are visible in the inner nacreous layer (Fig. S2.5 A–C) (55). This makes it unlikely that incorporation of atmospheric carbon is a significant source of contamination. Moreover, for the eastern Mediterranean, Boaretto et al. (51) see no relation between reservoir age and water depth or species (see also (56)). Precipitation of old carbon on rocky shore species by exposure to freshwater input from rivers in limestone or calcareous geological settings is another potential source of contamination (57). Limestone substrates do occur in the Lebanese coast and hinterland where Ksâr 'Akil is located. *P. turbinatus* is less tolerant to temperature and salinity changes than other species of the genus living in the Eastern Mediterranean (58, 59). As a result, it lives relatively low in the intertidal zone and is only found in rock pools that are regularly flushed out by seawater (21, 22, 59), avoiding localities where freshwater rivers or streams flow into the sea (59). We therefore assume that so-called hard-water effects do not have a major influence on the carbonate composition of *P. turbinatus.* Precipitation of old carbon onto shells after deposition in the rock shelter sediments could also occur and would result in a superficial diagenetic alterations and/or a carbonate crust adhering to the shells surface. Both the Oxford and Groningen pre-treatment protocols chemically etch the outer surface of the samples to remove these potential secondary carbonates.

In addition, it has been suggested that mollusks that graze on rocky shores may incorporate old carbon from the substrate while foraging (60–62). Small rock particles including old carbon can be abraded by the radulae of mollusks and are subsequently ingested with its food. This phenomenon may have affected radiocarbon dates on *Patella* spp. from the Iberian Peninsula, making them older that their true age (61). The radulae of the species used in our study, *Phorcus* sp., however, are described as "as soft as a brush" (i.e., Moh's scale 2.0–2.5), while radulae of *Patella* sp. are harder "like a shovel" (i.e., Moh's scale 4.0–4.5) (60, 63). Therefore, using *P. turbinatus* for dating reduces to a minimum the likelihood of obtaining older ages due to potential uptake of old carbon. Furthermore, fluctuations in ΔR values for intertidal rocky shore taxa measured in the eastern Mediterranean (i.e., *Patella caerulea* and *Phorcus* (*Osilinus*) *turbinatus*) are small, i.e., in the order of 200 years (33, 51). Calibration of our radiocarbon dates using either extreme ΔR value resulted in identical age estimations. As mentioned above, Boaretto et al. (51) found no correlation between δ^{13}C or ΔR values and water depth or shell environment, which would be observable when any of these potential ante-mortem contaminants played a significant role in carbonate biomineralization.
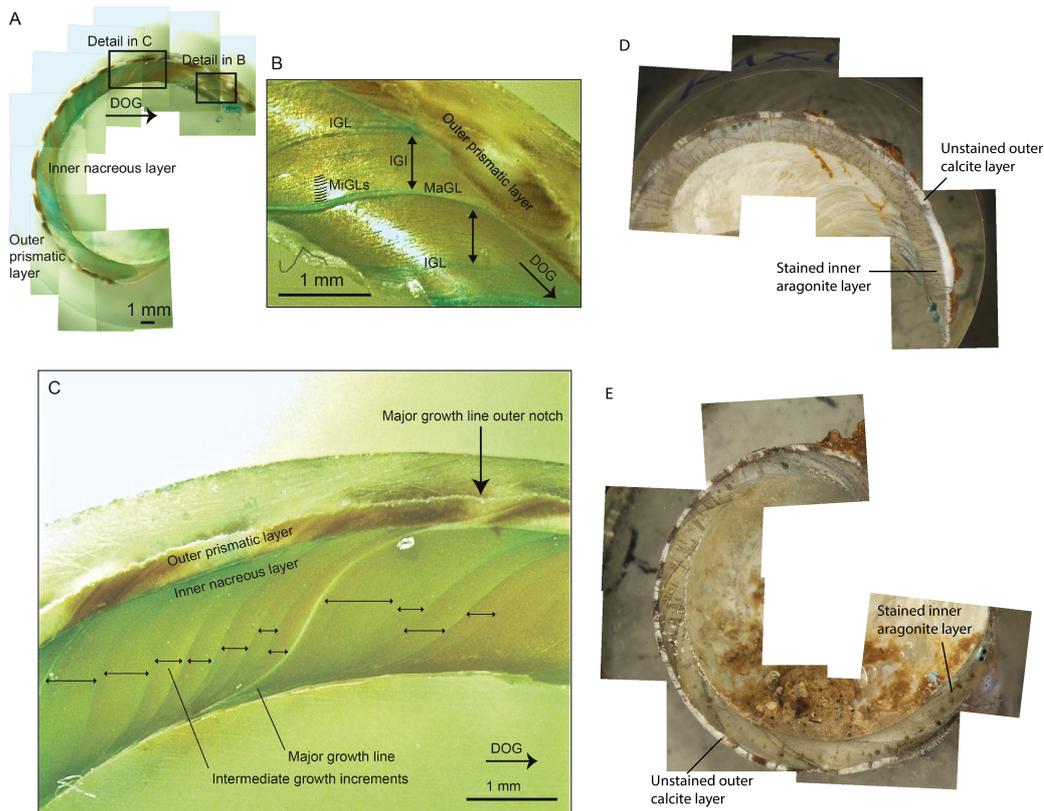
Figure S2.5. The microstructure of *Phorcus turbinatus* shell in cross section. The section is cut parallel to the direction of growth (DOG): A: Shell stained with Mutvei's solution to enhance visibility of growth increments. The whole outer whorl with outer prismatic later and inner nacreous layer is visible. B: Detail showing minor growth lines (MiGLs) deposited daily, intermediate growth increments (IGI) and intermediate growth lines (IGL) at fortnightly resolution, and a major growth line (MaGL) indicating an annual growth increment. C: Detail showing major growth line in the nacreous layer corresponding to major growth line outer notch in the prismatic layer. D and E: Shells from layer XI and XVII (1) respectively immersed in Feigl's solution for 20 minutes. The inner layers are stained grey indicating that they are aragonite whilst the outer layers remain unstained indicating that they are calcitic.

Pre-treatment method

In Groningen, the samples were cleaned in a 4% HCl bath, removing the outer surface chemically so that possible secondary carbonate is removed. From this pretreated shell fraction, CO_2 gas is produced using concentrated H_3PO_4 (64). Douka et al. (37) used the CarDS (39, 57) pretreatment protocol to eliminate potential contamination. The CarDS (carbonate density separation) method is aimed at separating the aragonitic and calcitic carbonate components of the shell using organic liquids (i.e., Bromoform by Russo et al. (57) or polytungstates by Douka et al. (39)). The method is based on the assumption that diagenetic alterations mainly result in the recrystallization of secondary calcite and that high magnesium calcite and aragonite are mainly in primary state. Only the aragonitic fraction is used for radiocarbon dating. It is expected that non-pretreated samples will give younger ages rather than older ones (but see (57)). For Ksâr 'Akil, Douka et al. (39) obtained two dates on sample number Ka 51 (Layer XXIII), one date without CarDS pretreatment (OxA-20489: 36,790 ± 270 BP) and one with CarDS (OxA-20490: 37,430 ± 320). The CarDS method effectively separated most calcite from the aragonite; the original sample had 80% calcite and the CarDS

sample 7%. The pretreatment method in this case results in a slightly older age, but overlaps with the non-pretreated sample at the 2σ level (see Table S2.3) (39). The non-pretreated sample is still ~4000 radiocarbon years younger than our date of Layer XXII (36,790 ± 270 years BP and 40,550 +350/-310 years BP, respectively). It is therefore unlikely that the CarDS pretreatment method causes these age discrepancies.

AMS radiocarbon laboratory

Both studies dated marine shells, but at different radiocarbon laboratories. The standard graphitization process and AMS protocols in both laboratories are practically identical. The CO_2 is reduced to C (graphite powder) by H_2 gas using Fe powder as a catalyst (65). The graphite powder is pressed into targets, which were placed in the sample carousel of the ion source of the AMS. The AMS system measured the isotopic ratios $^{14}C/^{12}C$ and $^{13}C/^{12}C$ of the graphite (66).

The dated event

The approach followed by both studies is similar in that it aims to date evidence of human activities as proxies for site occupation. Douka et al. (37) obtained their dates from ornamental shells with the objective of dating site occupation and "symbolically mediated" behavior (*sensu* (67)). We used *P. turbinatus,* brought to the site for consumption, to date shellfish exploitation and site occupation. However, our approaches differ when it comes to the time elapsed between the dated event and the so-called "target" event (68). The dated event is in both cases the time at which the ^{14}C was incorporated in the carbonate structure of the shell. Excepting post-mortem diagenetic changes, this occurs during shell growth i.e., during the life of the mollusk. The target event is what we want to date: the site occupation. With shell ornaments and tools, the mollusk may have been dead for a few years up to several millennia before the empty shell was collected by humans, whereas for consumed shellfish, death occurred at the site where the mollusk was eaten at the time of occupation. In addition, the "use-life" is also quite different. Given that the shells of *P. turbinatus* were likely discarded immediately after the mollusk had been consumed, their "use-life" would have been short and penecontemporaneous to site occupation. Empty shells, transformed into tools and ornaments, could have potentially been used for a relatively long time. By dating food remains, the dated event and target event are nearly identical, while in the case of shells used for utilitarian purposes, a gap of unknown duration exists between the death of the mollusk and its collection, as well as between its initial use and final deposition. Thus, we argue that dating molluskan species collected for consumption offers a more precise chronological estimate of site occupation. It also avoids dating shells that were subject to a marine taphonomic environment and inherent diagenetic changes as observed in macroscopic traces of decalcification of beached shells that were virtually absent in live-gathered taxa.

In summary, when radiocarbon dating shell carbonates, potential contamination with foreign carbon cannot be excluded. The main sources of contamination and the hardest to eliminate are post-mortem diagenetic processes that alter the mineral structure of shells. Methods for detecting diagenesis (e.g., macroscopic observations, Feigl solution, XRD), however useful, do not reveal potential carbon contamination by secondary aragonite, nor does the CarDS pretreatment method eliminate it. The effect of contamination by admixture with younger carbon increases with sample age and has a greater impact on AMS dates than on conventional dates (69). Therefore, it is preferable to date other organic materials (i.e., bone or charcoal) if available. In instances where such material is not available or poorly preserved, we argue it is essential to date the best-preserved

shells and taxa with the least evidence and/or likelihood of taphonomic alterations. In addition, dating species collected for consumption reduces the time elapsed between the life of the mollusk (i.e., the dated event) and the time of deposition (i.e., target event) and thereby provides us with a more precise chronological estimate of human presence at the site. In this study, we used a range of methods for assessing the diagenetic integrity of the samples, including XRD, staining with Feigl solution (see Fig. S2.5 D and E for examples), and biomolecular techniques (AAR) for evaluating closed-system behavior of the intra-crystalline proteins retained in the shell. The reasons for the discrepancies between the Douka et al. (37) chronology are currently unresolved, however the graphitization and AMS measurement methods at Groningen and Oxford are nearly identical and it is unlikely that either of those causes the differences observed. Ante-mortem incorporation of old carbon during grazing is unlikely due to the softness of *P. turbinatus* radulae, as is incorporation of atmospheric carbon while it is out of the water due to the species' behavior in these stressful periods. Local fluctuations of the reservoir effect in the eastern Mediterranean and the range of ΔR values for various intertidal rocky shore taxa are small and do not seem to influence the calibration results. Both the Groningen and Oxford pretreatment protocol use chemical cleaning to remove potential contamination by secondary carbonates. Post-mortem alterations generally make shell seem younger as they record the time of $\delta^{14}C$ substitution. We used best preserved shell displaying the least evidence for diagenetic alterations, whereas Douka et al. (37) used shell with macroscopically visible diagenetic alterations (38). Diagenetic processes are not fully understood and in the light of the recently proposed aragonite – aragonite substitutions (27) it seems plausible that the CarDS method did not successfully eliminate all contaminants. We therefore argue that our older radiocarbon dates provide more accurate estimates of the true sample ages.

Intra-crystalline protein diagenesis (Amino Acid Racemization, AAR)

Introduction

Mollusk shells are biocomposites containing a fraction of proteins and other organics that play a role in the biomineralization process during the organism's life (70). Protein diagenesis is a complex network of breakdown reactions that occur after death: these include peptide bond hydrolysis, racemization, and amino acid decomposition (e.g., dehydration of serine to alanine). The rate of diagenesis is temperature- and time-dependent and provided that the effect of other environmental and taphonomic factors can be excluded or accounted for, the extent of breakdown can be used as a proxy for estimating relative age since death. Historically, the main diagenesis reaction used for geochronological purposes has been amino acid racemization (AAR), the interconversion between the L- and D- enantiomers of an amino acid, yielding a D/L value between 0 (in live organisms) and 1 (when the reaction has reached equilibrium in old fossil shells).

Recent advances in the method (71) emphasized that the isolation of an intra-crystalline fraction of proteins by strong oxidation (bleaching) offers a more robust system for geochronological applications, as this intra-crystalline fraction is shown to behave as a "closed system" in a range of biominerals, including some species of mollusk shells (71–75). Protein geochronology has its main application over the Quaternary, due to lack of resolution over younger timescales (e.g., compared to radiocarbon). However, a big advantage of the new methodology is that the analysis of multiple amino acids and two different fractions of amino acids (Total Hydrolysable Amino Acids, THAA, and Free Amino Acids, FAA) allows identification of potentially compromised samples (75–77).

Method

Phorcus turbinatus samples were prepared and analyzed at the NEaar (North East Amino Acid Racemization) facility at the University of York (UK). Bleaching and leaching (high-temperature) experiments to test the suitability of *P. turbinatus* for the new method of AAR dating were undertaken as part of a larger study and confirmed that *P. turbinatus* retains a stable fraction of intra-crystalline proteins, which behaves as a closed system under artificial diagenesis conditions. Sample preparation for this study followed a standard protocol, which includes a 48-h bleaching step to isolate the intra-crystalline fraction, as detailed for other mollusk taxa (71, 74). Amino acid analyses were performed by liquid chromatography (RP-HPLC) following the method of Penkman et al. (71). This allows the detection of the L- and D- enantiomers of 10 amino acids. Here, we focus on the amino acids Asx (aspartic acid/asparagine), Glx (glutamic acid/glutamine), Ala (alanine), and Val (valine).

AAR analyses were undertaken on 26 *P. turbinatus* shell specimens, of which 13 had been dated by radiocarbon. A single AAR sample was taken from 23 specimens, and 2 samples (biological replicates) were obtained from 3 specimens (KSAS11XII, KSAS10XVI and KSAS09XVIII), for a total of 29 individual AAR samples (NEaar ID, Table S2.8). Each AAR sample was split into two subsamples for the analysis of the THAA and FAA fractions (71), and each subsample was analyzed twice by RP-HPLC (analytical replicates). Procedural blanks and standard amino acid mixtures of known D/L and concentration were interspersed during each analytical run.

Results

Table S2.8. D/L values of hydrolyzed (THAA) and free (FAA) amino acids. Results are presented as the average and standard deviation of two analytical replicates for each sample. KSA ID is the reference number for the current study. NEaar ID is the reference number for the amino acid racemization analysis at the NEaar laboratory (University of York).

KSA ID	NEaar ID	Fraction	Asx D/L		Glx D/L		Ala D/L		Val D/L	
			Av	σ	av	σ	Av	σ	Av	σ
KSASV04	8700bF	FAA	0.633	0.003	0.515	0.001	0.670	0.002	0.256	0.011
KSASV04	8700bH*	THAA	0.440	0.004	0.300	0.002	0.435	0.005	0.129	0.006
KSASV03	8701bF	FAA	0.687	0.004	0.573	0.098	0.713	0.007	0.256	0.013
KSASV03	8701bH*	THAA	0.516	0.002	0.292	0.004	0.503	0.002	0.143	0.001
KSASV02	8702bF	FAA	0.640	0.000	0.661	0.010	0.667	0.001	0.289	0.003
KSASV02	8702bH*	THAA	0.417	0.001	0.299	0.024	0.405	0.001	0.124	0.006
KSASV01	8703bF	FAA	0.670	0.011	0.546	0.049	0.700	0.003	0.237	0.006
KSASV01	8703bH*	THAA	0.483	0.012	0.311	0.028	0.514	0.008	0.132	0.007
KSAS01V	8704bF	FAA	0.686	0.001	0.604	0.005	0.708	0.001	0.248	0.001
KSAS01V	8704bH*	THAA	0.495	0.006	0.292	0.045	0.513	0.002	0.135	0.005
KSASVI04	8695bF	FAA	0.754	0.002	0.586	0.015	0.784	0.000	0.240	0.001
KSASVI04	8695bH*	THAA	0.591	0.000	0.353	0.002	0.664	0.010	0.167	0.001
KSASVI03	8696bF	FAA	0.681	0.001	0.623	0.078	0.674	0.006	0.248	0.002
KSASVI03	8696bH*	THAA	0.488	0.001	0.273	0.004	0.480	0.003	0.144	0.002
KSASVI02	8697bF	FAA	0.586	0.003	0.782	0.010	0.793	0.002	0.819	0.030
KSASVI02	8697bH*	THAA	0.406	0.000	0.408	0.003	0.532	0.012	0.241	0.007
KSASVI01	8698bF	FAA	0.644	0.007	0.565	0.030	0.687	0.009	0.251	0.013
KSASVI01	8698bH*	THAA	0.477	0.005	0.278	0.002	0.485	0.004	0.132	0.001
KSAS08VI	8699bF	FAA	0.614	0.011	0.611	0.156	0.641	0.002	0.249	0.011
KSAS08VI	8699bH*	THAA	0.446	0.007	0.267	0.029	0.441	0.003	0.118	0.000
KSASXI02	8692bF	FAA	0.734	0.014	0.576	0.026	0.789	0.003	0.254	0.009
KSASXI02	8692bH*	THAA	0.552	0.005	0.362	0.011	0.662	0.002	0.173	0.006
KSASXI01	8693bF	FAA	0.681	0.005	0.519	0.008	0.717	0.008	0.226	0.025
KSASXI01	8693bH*	THAA	0.494	0.000	0.291	0.009	0.529	0.009	0.135	0.001
KSAS02XI	8694bF	FAA	0.660	0.011	0.580	0.088	0.696	0.007	0.268	0.013
KSAS02XI	8694bH*	THAA	0.474	0.005	0.302	0.026	0.504	0.005	0.141	0.007
KSAS11XII	9344bF	FAA	0.631	0.001	0.456	0.003	0.712	0.000	0.251	0.002
KSAS11XII	9344bH*	THAA	0.479	0.001	0.271	0.001	0.511	0.001	0.139	0.000

Table S2.8. continued

KSA ID	NEaar ID	Fraction	Asx D/L		Glx D/L		Ala D/L		Val D/L	
			Av	σ	av	σ	Av	σ	Av	σ
KSAS11XII	9345bF	FAA	0.652	0.009	0.450	0.010	0.718	0.006	0.247	0.001
KSAS11XII	9345bH*	THAA	0.488	0.001	0.277	0.002	0.531	0.001	0.144	0.001
KSASXVI04	8687bF	FAA	0.729	0.003	0.559	0.052	0.815	0.005	0.224	0.015
KSASXVI04	8687bH*	THAA	0.572	0.000	0.355	0.009	0.704	0.016	0.190	0.013
KSASXVI03	8688bF	FAA	0.693	0.002	0.508	0.049	0.705	0.017	0.262	0.021
KSASXVI03	8688bH*	THAA	0.505	0.005	0.297	0.027	0.544	0.002	0.146	0.006
KSASXVI02	8689bF	FAA	0.719	0.010	0.531	0.020	0.734	0.014	0.272	0.021
KSASXVI02	8689bH*	THAA	0.532	0.002	0.335	0.004	0.578	0.002	0.181	0.022
KSASXVI01	8690bF	FAA	0.710	0.013	0.502	0.048	0.769	0.001	0.253	0.001
KSASXVI01	8690bH*	THAA	0.555	0.003	0.341	0.001	0.631	0.001	0.173	0.001
KSAS07XVI	8691bF	FAA	0.728	0.012	0.535	0.042	0.753	0.008	0.245	0.009
KSAS07XVI	8691bH*	THAA	0.571	0.006	0.342	0.012	0.663	0.010	0.179	0.006
KSAS10XVI	9346bF	FAA	0.599	0.001	0.451	0.003	0.663	0.000	0.270	0.003
KSAS10XVI	9346bH*	THAA	0.459	0.001	0.235	0.000	0.427	0.000	0.123	0.000
KSAS10XVI	9347bF	FAA	0.604	0.000	0.444	0.016	0.669	0.001	0.273	0.006
KSAS10XVI	9347bH*	THAA	0.462	0.001	0.241	0.001	0.448	0.002	0.131	0.004
KSASXVII03	8682bF	FAA	0.714	0.000	0.470	0.001	0.750	0.008	0.241	0.010
KSASXVII03	8682bH*	THAA	0.542	0.008	0.321	0.002	0.608	0.005	0.169	0.007
KSASXVII02	8683bF	FAA	0.665	0.005	0.348	0.005	0.697	0.000	0.262	0.011
KSASXVII02	8683bH*	THAA	0.480	0.001	0.240	0.007	0.498	0.015	0.147	0.010
KSASXVII01	8684bF	FAA	0.564	0.001	0.512	0.084	0.639	0.009	0.373	0.003
KSASXVII01	8684bH*	THAA	0.390	0.001	0.240	0.000	0.385	0.004	0.103	0.004
KSAS06XVII	8685bF	FAA	0.670	0.004	0.346	0.012	0.744	0.004	0.270	0.019
KSAS06XVII	8685bH*	THAA	0.486	0.004	0.276	0.004	0.594	0.017	0.158	0.000
KSAS03XVII	8686bF	FAA	0.694	0.001	0.439	0.004	0.701	0.004	0.223	0.005
KSAS03XVII	8686bH*	THAA	0.487	0.000	0.276	0.002	0.536	0.000	0.141	0.001
KSAS09XVIII	9348bF	FAA	0.667	0.000	0.455	0.005	0.705	0.001	0.241	0.003
KSAS09XVIII	9348bH*	THAA	0.514	0.000	0.288	0.000	0.541	0.003	0.159	0.001
KSAS09XVIII	9349bF	FAA	0.624	0.010	0.457	0.001	0.695	0.000	0.243	0.001
KSAS09XVIII	9349bH*	THAA	0.492	0.001	0.275	0.002	0.516	0.000	0.137	0.001

Closed-system behavior

Plots of THAA D/L versus FAA D/L values and THAA D/L versus THAA D/L values were used to assess the closed-system behavior of the samples analyzed. If the proteins analyzed (and their degradation products) are endogenous and have been undergoing diagenesis in a closed-system environment, then the two independent measures should be highly correlated, with compromised samples falling outside the trajectory of covariance (75, 77, 78). Typically, compromised samples are those where recrystallization of the mineral phase has occurred during diagenesis, and thus the intra-crystalline (closed) system might have incorporated exogenous amino acids or, more generally, the proteins

might have been affected by local fluctuations of pH or other environmental factors (open-system behavior).

P. turbinatus samples from Ksâr 'Akil showed excellent closed-system behavior (Fig. S2.6, A–D: covariance between THAA and FAA fractions of the same amino acid; Fig. S2.6, E–F: covariance between THAA D/Ls of two different amino acids). Glx FAA D/Ls are variable due to the difficulty of detecting FAA Glx, as this amino acid is preferentially released as stable lactam. One exception is represented by sample NEaar 8697, which falls outside the main trajectory of diagenesis for all amino acids except Asx, thus suggesting open-system behavior for this sample (Fig. S2.6). However, this shell was not analyzed for AMS dating (Table S2.1) and therefore this result does not affect the interpretation of the radiocarbon chronology of the site.

Sample NEaar 8684 taken from *Phorcus turbinatus* specimen XVII (3) corresponds to ^{14}C date GrA-57602, a potential outlier (see section on AMS dates). Although not as clear an outlier as sample NEaar 8697, it falls at the lower boundary of the D/L distribution for Asx and Ala (Fig. S2.6 A,C,E,F) and outside the main distribution on a Val THAA versus FAA plot, although variable FAA Val D/L values are to be expected as the result of low FAA concentrations of the D-enantiomer (74).
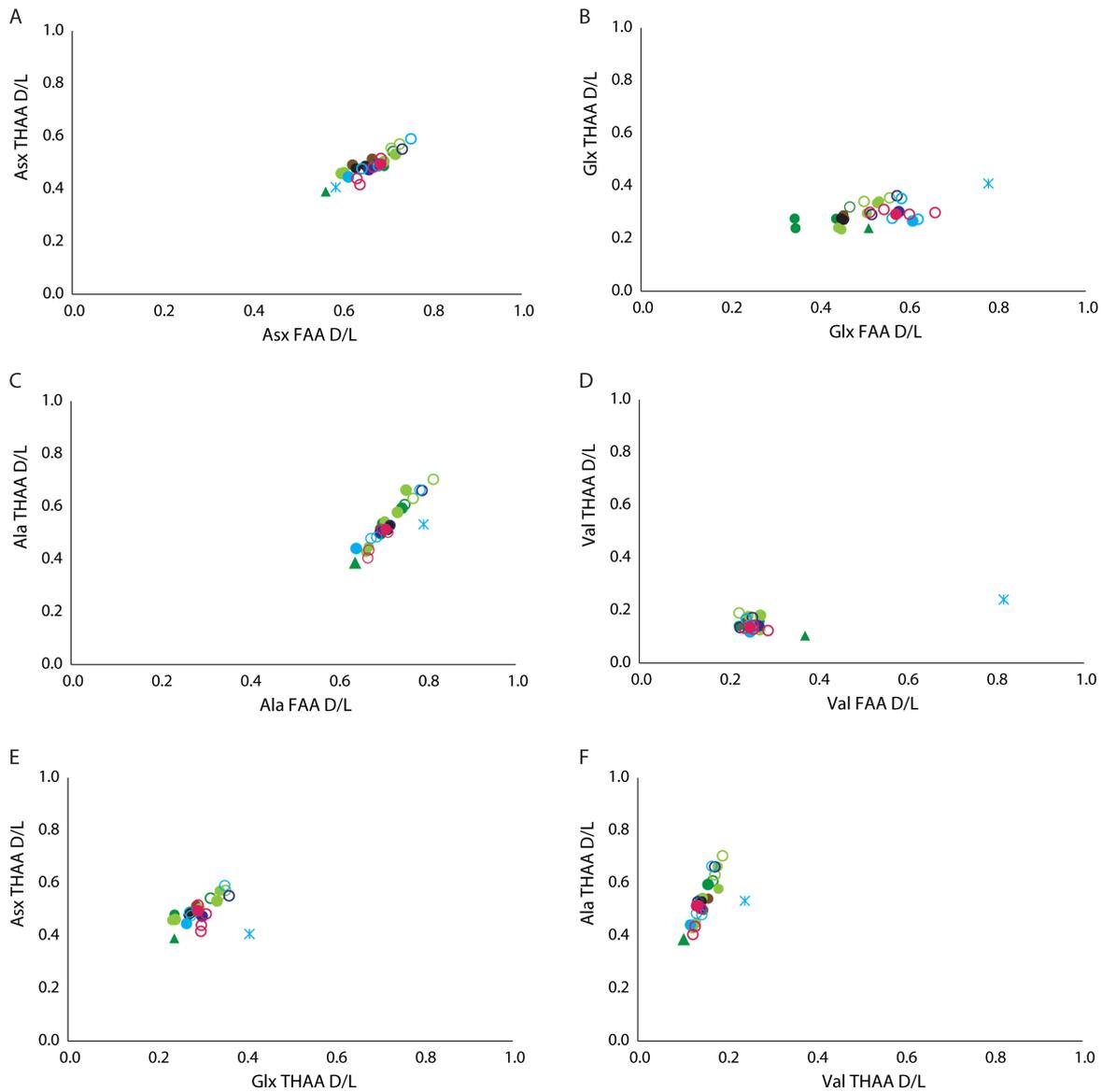
Figure S2.6. THAA vs FAA D/L plots for Asx (A), Glx (B), Ala (C), Val (D) and THAA vs THAA D/L plot for Asx vs Glx (E) and Ala vs Val (F). Note that most samples fall within a clearly defined trajectory of diagenesis, while sample 8697 is clearly highlighted as an outlier.

Natural variability

THAA D/L values for Asx, Glx, Ala, and Val show that the intra-layer variability (calculated as coefficient of variation, CV) is comparable to the overall site variability (Fig. S2.7). CVs of ~20% may be expected at site level, as recently found on a study on the intra-crystalline diagenesis of *Glycymeris* sp. in Mediterranean Last Interglacial raised beaches (75). Consequently, the resolution level of the method at this timescale (layers V–XVII, ca. 30–43 ka BP) is not sufficient to differentiate archeological layers and we did not attempt to use D/L values to resolve within-site ages.

Overall, the consistency of the AAR dataset supports no or very limited diagenetic post-depositional alteration for the shells analyzed in this study and used for radiocarbon and isotope analyses.
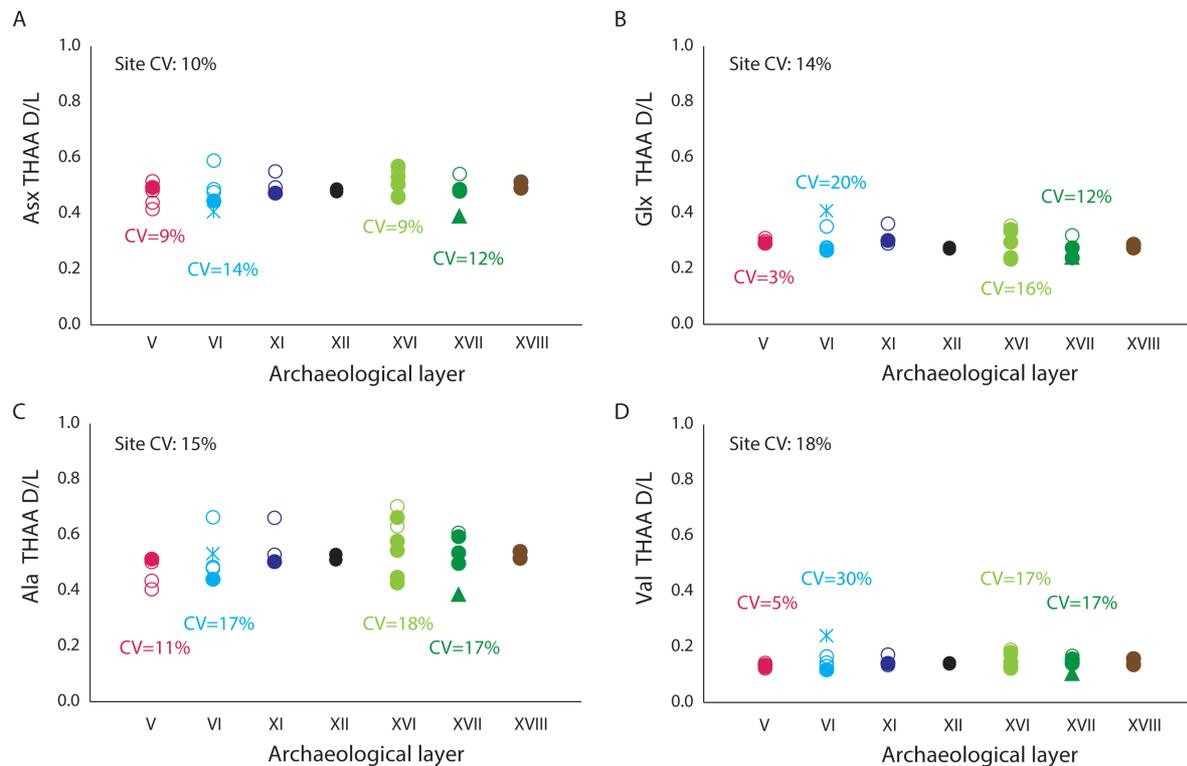

Figure S2.7. THAA D/L values for Asx (A), Glx (B), Ala (C) and Val (D) for each of the archeological layers considered in the AAR study. Radiocarbon-dated samples are represented by full circles. Potentially compromised samples are shown as triangle and cross. Note that the CVs for layers where the number of samples (n) is >5 is comparable to the CVs for the site, thus hampering resolution between layers.

Oxygen isotope analysis

Method

Oxygen isotope analysis was conducted on 13 specimens that were also dated with AMS radiocarbon and analyzed for AAR. Sampling was carried out at the Max Planck Institute for Evolutionary Anthropology. The sampling method was adopted after Mannino et al. (21) for *P. turbinatus*. A sequence of up to 40 samples was taken starting from the edge of the aperture along the periphery of the shell to obtain a full annual range of $\delta^{18}O$ values (Fig. S2.8). Sequential samples were taken from the midpoint of the aperture, because here the growth rate is highest and growth increments largest, thereby resulting in the least time-averaged results (21). The inner nacreous layer was sampled for oxygen isotope analyses, to avoid potential diagenesis, which is likely to have been most extensive in the outer prismatic layer, and because diagenetic alterations are more easily detectable in the aragonitic part of the shell (26). Therefore, the outer calcareous layer of the shell was initially removed with a hand drill along the periphery of the body whorl exposing the translucent nacreous layer. Then samples of carbonate powder (approximately 100 µg) were taken from the groove using a 0.5 mm drill bit. Care was taken to sample at equal depth at roughly 0.8-mm intervals starting at the midpoint of the aperture and continuing along the body whorl. Oxygen

isotope analyses were undertaken at the Godwin Laboratory for Palaeoclimatic Research, University of Cambridge. Carbonate samples were transferred to exetainer vials and sealed with silicone rubber septa using a screw cap. The samples were flushed with CP grade helium, then acidified, left to react for 1 h at 70°C and then analyzed using a Thermo Gasbench preparation system attached to a Thermo MAT 253 mass spectrometer in continuous flow mode. Each run of samples was accompanied by 10 reference carbonates (Carrara Z) and two control samples (Fletton Clay). Carrara Z has been calibrated to the Vienna Pee Dee Belemite (VPDB) using the international standard NBS19. Results are reported in delta units (δ) in parts per mil (‰) with reference to the international VPDB standard and the precision is better than ± 0.10 ‰ for $\delta^{18}O$.
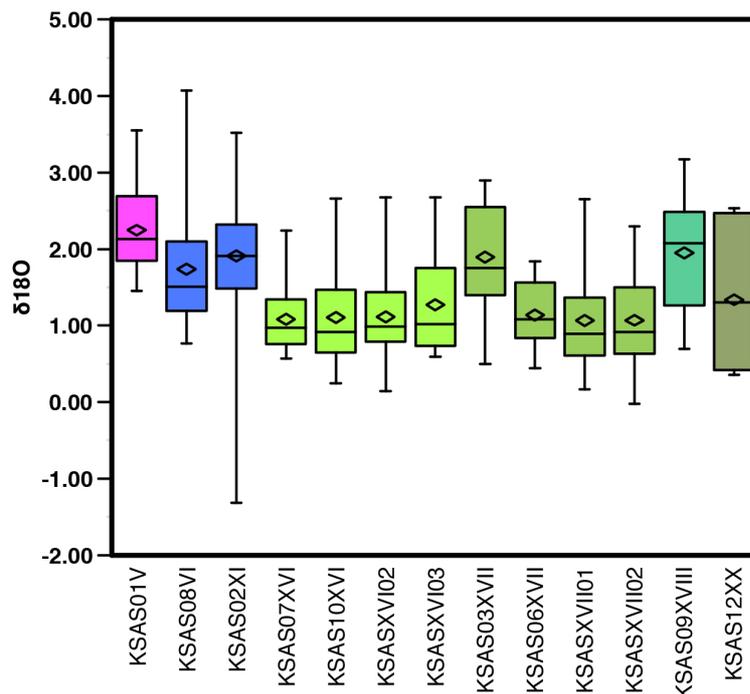

Figure S2.8. Boxplots showing ranges of $\delta^{18}O$ values in per mil (‰) for *P. turbinatus* per selected specimen. Early Upper Paleolithic (EUP): green, Upper Paleolithic (UP): blue, Epipaleolithic (EPI): pink. Boxes show the range of data points between the 25th and 75th percentile. Whiskers include extreme data points. Also shown are the median (horizontal bar) and mean (diamond) values.
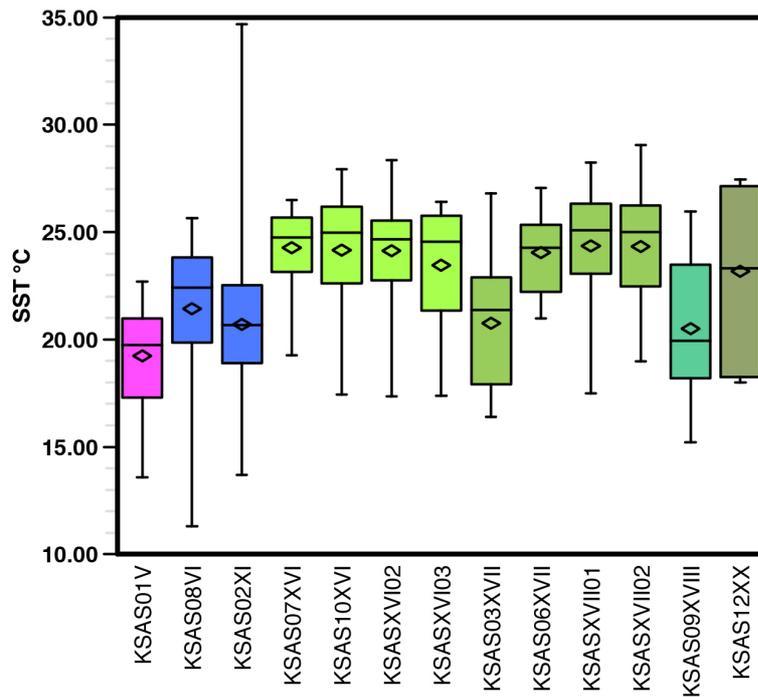
Figure S2.9 Boxplots showing ranges of sea surface temperature (SST) values in degrees Celsius (°C) for *P. turbinatus* per selected specimen. Early Upper Paleolithic (EUP): green, Upper Paleolithic (UP): blue, Epipaleolithic (EPI): pink. Boxes show the range of data points between the 25th and 75th percentile. Whiskers include extreme data points. Also shown are the median (horizontal bar) and mean (diamond) values.

The obtained $\delta^{18}O$ values were used to calculate SST estimates using the established aragonite-temperature equations of Grossman and Ku (79) with a conversion of VSMOW (used for $\delta^{18}O_{water}$ values) to VPDB by Dettman et al. (80) (Table S2.9; Fig. S2.9). Mollusk shell $\delta^{18}O$ is a function of the $\delta^{18}O$ of ambient water ($\delta^{18}O_{water}$) and temperature (80). For paleotemperature reconstruction an estimation of paleo $\delta^{18}O_{water}$ must be incorporated in the equation. Here, we used measured mean annual $\delta^{18}O_{water}$ values of 1.2‰ from a modern calibration study in Libya and incorporated an estimated correction for the glacial conditions during MIS 3. Paul et al. (81) showed that Mediterranean sea $\delta^{18}O_{water}$ was higher by 1.2‰ during the last glacial based on $\delta^{18}O$ pore water of Mediterranean marine sediment cores. The fact that the Ksâr 'Akil shells do not date to the height of the LGM introduces some unknown error into the SST calculations, as $\delta^{18}O_{water}$ fluctuated quite substantially during MIS 3. However, at this stage no other independent paleothermometers exist to compare with the $\delta^{18}O_{shell}$ analysis to provide a better understanding of local and temporal $\delta^{18}O_{water}$ fluctuations. Here, we used an approximation of sea $\delta^{18}O$ during MIS 3 of 1.0‰. This resulted in the following equation: SST°C = 20.6–4.34 ($\delta^{18}O_{shell\ (VPDB)}$ – (2.2–0.27)). Although the SST estimates might not be entirely accurate, our approximation allows evaluation of the relative differences in SST between shells and between archeological layers.

Table S2.9. Oxygen isotope analysis and Sea Surface Temperature estimates. KSA nr: sample ID; n: number of sequential samples; min: minimum $\delta^{18}O_{shell}$ value; max: maximum $\delta^{18}O_{shell}$ value; mean: mean $\delta^{18}O_{shell}$; SD: Standard deviation; range: range of $\delta^{18}O_{shell}$ values; SST rec: Paleo Sea Surface Temperature estimates in °C using the equation mentioned in the text (79–81).

KSA nr	n of samples	Min ($\delta^{18}O_{shell}$)	Max ($\delta^{18}O_{shell}$)	Mean ($\delta^{18}O_{shell}$)	SD ($\delta^{18}O_{shell}$)	Range ($\delta^{18}O_{shell}$)	SST rec (°C)
KSAS01V	40	1.45	3.55	2.25	0.57	2.10	19.2
KSAS08VI	40	0.77	4.07	1.74	0.80	3.30	21.4
KSAS02XI	40	0.51	3.52	1.91	0.84	3.01	20.7
KSAS07XVI	32	0.57	2.24	1.08	0.39	1.67	24.3
KSAS10XVI	35	0.24	2.66	1.11	0.60	2.42	24.2
KSASXVI02	40	0.15	2.68	1.11	0.56	2.53	24.1
KSASXVI03	30	0.59	2.67	1.27	0.62	2.08	23.5
KSAS03XVII	36	0.50	2.90	1.90	0.80	2.40	20.8
KSAS06XVII	30	0.44	1.84	1.14	0.42	1.40	24.0
KSASXVII01	30	0.17	2.65	1.07	0.59	2.48	24.4
KSASXVII02	40	0.29	2.30	1.07	0.56	2.01	24.3
KSAS09XVIII	40	0.70	3.17	1.95	0.67	2.47	20.5
KSAS12XX	15	0.35	2.53	1.34	0.86	2.18	23.2

These SST estimates were compared to present-day conditions (~23°C from AVHRR data for offshore Lebanon (82) and temperature estimations for Marine Isotope Stage 3 (83, 84)). Samples V, VI, XI, and XVII (1), and XVIII show comparably low mean annual SST values, ranging from 19.2°C to 21.4°C, and represent cooler phases throughout the Ksâr 'Akil sequence. Warmer mean annual SSTs ranging between 23.2–24.4°C are represented by samples XVI (1–4), XVII (2–4), and XX.

Section 3: Comparison with early UP sites and human fossils

Early Upper Paleolithic sites

Table S3.1. Early Upper Paleolithic sites in Europe and the Levant mentioned in the text. IUP = Initial Upper Paleolithic; EUP = Early Upper Paleolithic; Proto-Aur = Proto-Aurignacian. Calibrated radiocarbon dates given at 68.2% probability level, * = weighted mean for TL dates (in years ago). ' = calibrated/modeled with Marine13; " = calibrated with IntCal13 (charcoal) and Marine13 (shell); ^ = calibrated with IntCal13; ~ = calibrated/modeled with Marine09. IntCal/Marine13 (31); IntCal/Marine09 (85).

site [country]	technocomplex	layer	Method	date cal BP (68.2%)	reference
Ksâr 'Akil	IUP	XXII	^{14}C	44,580–43,180'	this paper
Boker Tachtit [Israel]	IUP	1–4	^{14}C	>50,000–40,000	(86)
Üçağızlı I [Turkey]	IUP	I–F	^{14}C	45,890–37,060"	(15)
Manot [Israel]	IUP	area C Unit 7	^{14}C	>50,000	(87)
Üçağızlı I [Turkey]	EUP	E–B	^{14}C	42,840–32,180"	(15)
Ksâr 'Akil	EUP	XX–XIV	^{14}C	43,270–42,760'	this paper
Kebara Cave [Israel]	EUP	Units III–IV	^{14}C	46,000–34,000	(88)
Manot Cave [Israel]	EUP	area C Unit 7	^{14}C	46,000–42,000	(89)
Isturitz [France]	Proto-Aur	C4c4	^{14}C	42,300–41,700^	(90)
Riparo Mochi [Italy]	Proto-Aur	G	^{14}C	42,700–41,600~	(91)
Românești-Dumbrăviţa I [Romania]	Proto-Aur	GH3	TL	42,100–39,100*	(92)
Brno-Kejbaly [Czech Republic]	Bohunician	base Bohunice soil	^{14}C	47,410–44,420	(93)
Brno-Bohunice 2002 [Czech Republic]	Bohunician	Bohunice soil	TL	50,000–46,300*	(94)

Human fossils

Table S3.2. Human fossil remains mentioned in the text. IUP = Initial Upper Paleolithic. Method: laboratory number indicates a direct date; range: range of dates for the layer(s) from which the fossil(s) originate; PDF = modeled date for specimen. Calibrated dates given at 68.2% probability level. ' = calibrated /modeled with Marine13; ~ = calibrated/modeled with Marine09; * = average corrected age (arithmetic mean ±2σ), " = Calibrated with a combination of IntCal13/Marine13; ^ = Calibrated with IntCal13. IntCal/Marine13 (31); IntCal/Marine09 (84).

site [fossil]	layer	technocomplex	method	date cal BP (68.2%)	reference
Ksâr 'Akil [Egbert]	XVII	Ahmarian	^{14}C (PDF)	43,270–42,760'	this paper
Ksâr 'Akil [Ethelruda]	XXV	IUP	^{14}C (PDF)	> 45,870'	this paper
Cavallo [C]	E II–I	Uluzian	^{14}C (PDF)	44,000–43,000~	(95)
Cavallo [B]	E III	Uluzian	^{14}C (PDF)	45,010–43,380~	(95)
Manot [1]	na	no archeology	uranium-thorium	60,200–49,200*	(87)
Peştera cu Oase [1]	na	no archeology	^{14}C (GrA-22810)	40,040–37,610"	(96)
Üçağızlı I [6 teeth]	B–E	Ahmarian	^{14}C (range)	42,840–32,180"	(41, 97, 98)
Üçağızlı I [3 teeth]	F	IUP	^{14}C (range)	40,360–37,060"	(42, 97, 98)
Üçağızlı I [1 tooth]	H–I	IUP	^{14}C (range)	45,890–37,800"	(42, 97, 98)
Kostenki 14 [tooth]	IVb	unnamed IUP	^{14}C (GrA-15961)	41,490–40,920^	(99, 100)
Kostenki 14 [skeleton]	burial	no archeology	^{14}C (OxA-X-2395-15)	38,210–36,820^	(101)
Kostenki 1 [tibia & fibula]	III	Aurignacian	^{14}C (OxA-15055)	36,200–35,760^	(102, 103)
Kostenki 17 [tooth]	II	Spitsynian	^{14}C (GrN-12596)	42,800–39,700^	(104)
Ust'-Ishim [femur]	na	no archeology	^{14}C (range)	46,200–43,600^	(105)

References

1. Ewing FJ (1947) Preliminary note on the excavations at the Palaeolithic site of Ksâr 'Akil, Republic of Lebanon. *Antiquity* 21(84):186–196.

2. Ewing JF (1948) Ksâr 'Akil in 1948. *Biblica* 29:272–278

3. Wright HE (1962) Late Pleistocene geology of coastal Lebanon. *Quaternaria* 6:525–539.

4. Bergman C, Azoury I, Seeden H (2012) Ksar Aqil: At the crossroads out of Africa. *Saudi Aramco World* 63:1–7.

5. Ewing JF (1949) The treasures of Ksâr 'Akil. *Thought* 24:255–288.

6. Mellars P, Tixier J (1989) Radiocarbon-accelerator dating of Ksar 'Aqil (Lebanon) and the chronology of the Upper Palaeolithic sequence in the Middle East. *Antiquity* 63:761–768.

7. Tixier J, Inizan M-L (1981) Ksar Aqil, stratigraphie et ensembles lithiques dans le Paléolithique Supérieur: fouilles 1971–1975. *Colloques Internationaux du CNRS* 598: 353–367.

8. Braidwood RJ, Wright HE, Ewing JF (1951) Ksâr 'Akil: its archeological sequence and geological setting. *Journal of Near Eastern Studies* 10(2):113–122.

9. Ewing JF (1960) Human types and prehistoric cultures at Ksâr 'Akil, Lebanon. *Men and Cultures: Selected Papers Fifth Int. Congr. Anthrop. Ethnol. Sci. Philadelphia* 1956:535–539.

10. Murphy JW (1938) The method of Prehistoric excavation at Ksâr 'Akil. *Anthropological series, Boston college graduate school* III:272–275.

11. Hooijer DA (1961) The fossil vertebrates of Ksâr 'Akil, a Palaeolithic rock shelter in the Lebanon. *Zoologische Verhandelingen* 49(1):1–68.

12. van Regteren Altena CO (1962) Molluscs and echinoderms from Palaeolithic deposits in the rock shelter of Ksâr'Akil, Lebanon. *Zoologische Mededelingen* 38(5):87–99.

13. Marks AE, Volkman P (1986) The Mousterian of Ksar Akil: levels XXVIA through XXVIIIB. *Paléorient* 12(1):5–20.

14. Williams JK, Bergman CA (2010) Upper Paleolithic levels XIII–VI (A and B) from the 1937–1938 and 1947–1948 Boston College excavations and the Levantine Aurignacian at Ksar Akil, Lebanon. *Paléorient* 36(2):117–161.

15. Kuhn SL, Stiner MC, Reese DS, Güleç E (2001) Ornaments of the earliest Upper Paleolithic: new insights from the Levant. *Proceedings of the National Academy of Sciences USA* 98(13):7641–7646.

16. Behrensmeyer AK (1978) Taphonomic and ecologic information from bone weathering. *Paleobiology* 4(2):150–162.

17. Stiner MC, Kuhn SL, Weiner S, Bar-Yosef O (1995) Differential burning, recrystallization, and fragmentation of archaeological bone. *Journal of Archaeological Science* 22(2):223–237.

18. Shea JJ (2003) The Middle Paleolithic of the east Mediterranean Levant. *Journal of World Prehistory* 17(4):313–394.

19. Douka K (2011) An Upper Palaeolithic shell scraper from Ksar Akil (Lebanon). *Journal of Archaeological Science* 38(2):429–437.

20. Stiner MC, Kuhn SL, Güleç E (2013) Early Upper Paleolithic shell beads at Üçağızlı Cave I (Turkey): technology and the socioeconomic context of ornament life-histories. *Journal of Human Evolution* 64(5):380–98.

21. Mannino MA, Thomas KD, Leng MJ, Sloane HJ (2008) Shell growth and oxygen isotopes in the topshell *Osilinus turbinatus*: resolving past inshore sea surface temperatures. *Geo-Marine Letters* 28(5–6):309–325.

22. Prendergast AL, Azzopardi M, O'Connell TC, Hunt C, Barker G, Stevens RE (2013) Oxygen isotopes from *Phorcus (Osilinus) turbinatus* shells as a proxy for sea surface temperature in the central Mediterranean: A case study from Malta. *Chemical Geology* 345:77–86.

23. Mannino MA, Thomas KD, Leng MJ, Piperno M, Tusa S, Tagliacozzo A (2007) Marine resources in the Mesolithic and Neolithic at the Grotta dell'Uzzo (Sicily): Evidence from isotope analyses of Marine shells. *Archaeometry* 49(1):117–133.

24. Mannino MA, Thomas KD (2007) New radiocarbon dates for hunter-gatherers and early farmers in Sicily. *Accordia Research Papers* 10:13–33.

25. Bosch DM, Mannino MA, Prendergast A, O'Connell TC, Wesselingh F, van der Plicht J, Hublin J-J (2013) Initial Upper Palaeolithic to Epi-Palaeolithic marine mollusc exploitation at Ksâr 'Akil (Lebanon): new zooarchaeological, radiometric, and isotopic data. *PaleoAnthropology Paleoanthropology Society Meetings Abstracts, Honolulu, HI, 2–3 April 2013:*A7

26. Kato K, Wada H, Fujioka K (2003) The application of chemical staining to separate calcite and aragonite minerals for micro-scale isotopic analyses. *Geochemical Journal* 37(2):291–297.

27. Busschers FS, Wesselingh F, Kars RH, Versluijs-Helder M, Wallinga J, Bosch JHA, Timmner J, Nierop KGJ, Meijer T, Bunnik FPM, De Wolf H (2014) Radiocarbon dating of Late Pleistocene marine shells from the southern North Sea. *Radiocarbon* 56(3):1151–1166.

28. Schöne BR, Dunca E, Fiebig J, Pfeiffer M (2005) Mutvei's solution: An ideal agent for resolving microgrowth structures of biogenic carbonates. *Palaeogeography, Palaeoclimatology, Palaeoecology* 228(1–2):149–166.

29. Feigl F (1958) *Spot tests in inorganic analysis* (Elsevier, Amsterdam).

30. Fenger T, Surge D, Schöne B, Milner N (2007) Sclerochronology and geochemical variation in limpet shells (*Patella vulgata*): a new archive to reconstruct coastal sea surface temperature. *Geochemistry, Geophysics, Geosystems* 8(7):1–17.

31. Reimer PJ, Bard E, Bayliss A, Beck JW, Blackwell PG, Ramsey CB, Buck CE, Cheng H, Edwards RL, Friedrich M, Grootes PM, Guilderson TP, Haflidason H, Hajdas I, Hatté C, Heaton TJ, Hoffman DL,

Hogg AG, Hughen KA, Kaiser KF, Kromer B, Manning SW, Niu M, Reimer RW, Richards DA, Scott EM, Southon JR, Staff RA, Turney CSM, van der Plicht J (2013) IntCal13 and Marine13 radiocarbon age calibration curves 0–50,000 years cal BP. *Radiocarbon* 55(4):1869–1887.

32. Bronk Ramsey C (2009) Bayesian analysis of radiocarbon dates. *Radiocarbon* 51(1):337–360.

33. Reimer PJ, McCormac FG (2002) Marine radiocarbon reservoir corrections for the Mediterranean and Aegean Seas. *Radiocarbon* 44(1):159–166.

34. Bergman CA, Goring-Morris AN (1987) Conference: The Levantine Aurignacian with special reference to Ksar Akil, Lebanon March 27–28, 1987 Institute of Archaeology, London. *Paléorient* 13(1):142–147.

35. Goring-Morris NA, Belfer-Cohen A (2003) *More than meets the eye: studies on Upper Palaeolithic diversity in the Near East* (Oxbow Books, Oxford).

36. Vogel JC, Waterbolk HT (1963) Groningen radiocarbon dates IV. *Radiocarbon* 5:163–202.

37. Douka K, Bergman CA, Hedges REM, Wesselingh FP, Higham T (2013) Chronology of Ksar Akil (Lebanon) and implications for the colonization of Europe by anatomically modern humans. *PLoS ONE* 8(9):e72931.

38. Ohnuma K, Bergman CA (1990) A technological analysis of the Upper Palaeolithic levels (XXV–VI) of Ksar 'Akil, Lebanon. *The emergence of modern humans: an archaeological perspective*, ed Mellars P (Edinburgh University, Edinburgh), pp 91–138.

39. Douka K, Hedges RM, Higham TG (2010) Improved AMS ^{14}C dating of shell carbonates using high-precision X-ray Diffraction and a novel density separation protocol (CarDS). *Radiocarbon* 52(2):735–751.

40. Bronk Ramsey C (2009) Dealing with outliers and offsets in radiocarbon dating. *Radiocarbon* 51(3):1023–1045.

41. Kuhn SL, Stiner MC, Güleç E, Özer I, Yilmaz H, Baykara I, Açikkol A, Goldberg P, Molina KM, Ünay E, Suata-Alpasian F (2009) The early Upper Paleolithic occupations at Üçağızlı Cave (Hatay, Turkey). *Journal of Human Evolution* 56:87–113.

42. Bergman CA, Stinger CB (1989) Fifty years after: Egbert, an Early Upper Palaeolithic juvenile from Ksar Akil, Lebanon. *Paléorient* 16(2):99–111.

43. Kowalewski M (1996) Time-averaging, overcompleteness, and the geological record. *The journal of Geology* 104:317–326.

44. Kowalewski M, Goodfriend GA, Flessa KW (1998) High-resolution estimates of temporal mixing within shell beds: the evils and virtues of time-averaging. *Paleobiology* 24(3):287–304.

45. Olszewski T (1999) Taking advantage of time-averaging. *Paleobiology* 25(2):226–238.

46. Sivan D, Potasman M, Almogi-Labin A, Bar-Yosef Mayer DE, Spanier E, Boaretto E (2006) The Glycymeris query along the coast and shallow shelf of Israel, southeast Mediterranean. *Palaeogeography, Palaeoclimatology, Palaeoecology* 233(1–2):134–148.

47. Nielsen JK, Funder S (2003) Taphonomy of Eemian marine molluscs and acorn barnacles from eastern Arkhangelsk region, northern Russia. *Palaeogeography, Palaeoclimatology, Palaeoecology* 191(2):139–168.

48. Mangerud J (1972) Radiocarbon dating of marine shells, including a discussion of apparent age of recent shells from Norway. *Boreas* 1(2):143–172.

49. Nadeau M-J, Grootes PM, Voelker A, Bruhn F, Duhr A, Oriwall A (2001) Carbonate ^{14}C background: does it have multiple personalities? *Radiocarbon* 43(2A):169–176.

50. Stuiver M, Braziunas TF (1993) Modeling atmospheric ^{14}C influences and ^{14}C ages of marine samples to 10,000 BC. *Radiocarbon* 35(1):137–137.

51. Boaretto E, Mienis HK, Sivan D (2010) Reservoir age based on pre-bomb shells from the intertidal zone along the coast of Israel. *Nuclear Instruments and Methods in Physics Research Section B: Beam Interactions with Materials and Atoms* 268(7–8):966–968.

52. Siani G, Paterne M, Arnold M, Bard E, Mativier B, Tisnerat N, Bassinot F (2000) Radiocarbon reservoir ages in the Mediterranean Sea and Black Sea. *Radiocarbon* 42(2):271–280.

53. Hogg AG, Higham TFG (1998) ^{14}C dating of modern marine estuarine shellfish. *Radiocarbon* 40(2):975–984.

54. Schöne BR (2008) The curse of physiology—challenges and opportunities in the interpretation of geochemical data from mollusk shells. *Geo-Marine Letters* 28(5–6):269–285.

55. Schöne BR, Rodland DL, Wehrmann A, Heidel B, Oschmann W, Zhang Z, Fiebig J, Beck L (2007) Combined sclerochronologic and oxygen isotope analysis of gastropod shells (*Gibbula cineraria*, North Sea): life-history traits and utility as a high-resolution environmental archive for kelp forests. *Marine Biology* 150(6):1237–1252.

56. Ascough PL, Cook GT, Dugmore AJ, Scott EM, Freeman SP (2005) Influence of mollusc species on marine ΔR determinations. *Radiocarbon* 47(3):433–440.

57. Russo CM, Tripp JA, Douka K, Higham TF (2010) A new radiocarbon pretreatment method for molluscan shell using density fractionation of carbonates in Bromoform. *Radiocarbon* 52(3):1301–1311.

58. Schifano G, Censi P (1983) Oxygen isotope composition and rate of growth of *Patella coerulea, Monodonta turbinata* and *M. articulata* shells from the western coast of Sicily. *Palaeogeography, Palaeoclimatology, Palaeoecology* 42(3):305–311.

59. Menzies R, Cohen Y, Lavie B, Nevo E (1992) Niche adaptation in two marine gastropods, *Monodonta turbiformis* and *M. turbinata*. *Bolletino di zoologia* 59(3):297–302.

60. Crothers JH (2001) Common topshells: an introduction to the biology of *Osilinus lineatus* with notes on other species in the genus. *Field Studies* 10:115–160.

61. Ferguson JE, Henderson GM, Fa DA, Finlayson JC, Charnley NR (2011) Increased seasonality in the Western Mediterranean during the last glacial from limpet shell geochemistry. *Earth and Planetary Science Letters* 308(3–4):325–333.

62. Dye T (1994) Apparent ages of marine shells: implications for archaeological dating in Hawai'i. *Radiocarbon* 36(1):51–57.

63. Hawkins SJ, Watson DC, Hill AS, Harding SP, Kyriakides MA, Hutchinson S, Norton TA (1989) A comparison of feeding mechanisms in microphagous, herbivorous, intertidal, prosobranchs in relation to resource partitioning. *Journal of Molluscan Studies* 55(2):151–165.

64. Mook WG, Streurman HJ (1983) Physical and chemical aspects of radiocarbon dating. *PACT* 8: 31–55.

65. Aerts-Bijma AT, van der Plicht J, Meijer HAJ (2001) Automatic AMS Sample Combustion and CO_2 Collection. *Radiocarbon* 43(2):293–298.

66. van der Plicht J, Wijma S, Aerts AT, Pertuisot MH, Meijer HAJ (2000) Status report: the Groningen AMS facility. *Nuclear Instruments and Methods in Physics Research Section B: Beam Interactions with Materials and Atoms* 172(1):58–65.

67. d'Errico F, Stringer CB (2011) Evolution, revolution or saltation scenario for the emergence of modern cultures? *Philosophical Transactions of the Royal Society of London B. Biological Sciences* 366:1060–1069.

68. Dean JS (1978) Independent dating in archaeological analysis. *Advances in Archaeological Method and Theory* 1:223–255.

69. van der Plicht J (2012) Borderline radiocarbon. *Netherlands Journal of Geosciences* 91(1–2):257–261.

70. Weiner S, Traub W, Parker SB (1984) Macromolecules in mollusc shells and their functions in biomineralization. *Philosophical Transactions of the Royal Society of London. B, Biological Sciences* 304(1121):425–434.

71. Penkman KEH, Kaufman DS, Maddy D, Collins MJ (2008) Closed-system behaviour of the intra-crystalline fraction of amino acids in mollusc shells. *Quaternary Geochronology* 3(1):2–25.

72. Penkman KEH, Preece RC, Bridgland DR, Keen DH, Meijer T, Parfitt SA, White TS, Collins MJ (2011) A chronological framework for the British Quaternary based on Bithynia opercula. *Nature* 476(7361):446–449

73. Demarchi B, Williams MG, Milner N, Russell N, Bailey G, Penkman K (2011) Amino acid racemization dating of marine shells: a mound of possibilities. *Quaternary International* 239(1):114–124.

74. Demarchi B, Rogers K, Fa DA, Finlayson CJ, Milner N, Penkman KEH (2013) Intra-crystalline protein diagenesis (IcPD) in *Patella vulgata*. Part I: isolation and testing of the closed system. *Quaternary Geochronology* 16:144–157.

75. Demarchi B, Clements E, Coltorti M, van de Locht R, Kröger R, Penkman K, Rose J (2015) Testing the effect of bleaching on the bivalve Glycymeris: a case study of amino acid geochronology on key Mediterranean raised beach deposits. *Quaternary Geochronology* 25:49–65.

76. Preece RC, Penkman KEH (2005) New faunal analyses and amino acid dating of the Lower Palaeolithic site at East Farm, Barnham, Suffolk. *Proceedings of the Geologists' Association* 116(3):363–377.

77. Penkman KE, Preece RC, Bridgland DR, Keen DH, Meijer T, Parfitt SA, White TS, Collins MJ (2013) An aminostratigraphy for the British Quaternary based on Bithynia opercula. *Quaternary science reviews* 61:111–134.

78. Kaufman DS (2006) Temperature sensitivity of aspartic and glutamic acid racemization in the foraminifera Pulleniatina. *Quaternary Geochronology* 1(3):188–207.

79. Grossman EL, Ku T-L (1986) Oxygen and carbon isotope fractionation in biogenic aragonite: temperature effects. *Chemical Geology: Isotope Geoscience section* 59:59–74.

80. Dettman DL, Reische AK, Lohmann KC (1999) Controls on the stable isotope composition of seasonal growth bands in aragonitic fresh-water bivalves (Unionidae). *Geochimica et Cosmochimica Acta* 63(7):1049–1057.

81. Paul HA, Bernasconi SM, Schmid DW, McKenzie JA (2001) Oxygen isotopic composition of the Mediterranean Sea since the Last Glacial Maximum: constraints from pore water analyses. *Earth and Planetary Science Letters* 192(1):1–14.

82. Kilpatrick KA, Podestá GP, Evans R (2001) Overview of the NOAA/NASA advanced very high resolution radiometer Pathfinder algorithm for sea surface temperature and associated matchup database. *Journal of Geophysical Research* 106(C5):9179–9197.

83. Sánchez Goñi M, Cacho I, Turon J, Guiot J, Sierro F, Peypouquet J, Grimalt J, Shackleton N (2002) Synchroneity between marine and terrestrial responses to millennial scale climatic variability during the last glacial period in the Mediterranean region. *Climate Dynamics* 19(1):95–105.

84. Svensson A, Andersen KK, Bigler M, Clausen HB, Dahl-Jensen D, Davies SM, Johnsen SJ, Muscheler R, Parrenin F, Rasmussen SO (2008) A 60 000 year Greenland stratigraphic ice core chronology. *Climate of the Past* 4(1):47–57.

85. Reimer PJ, Baillie MG, Bard E, Bayliss A, Beck JW, Blackwell PG, Ramsey CB, Buck CE, Burr GS, Edwards RL, Friedrich M, Grootes PM, Guilderson TP, Hajdas I, Heaton TJ, Hogg AG, Hughen KA, Kaiser KF, Kormer B, McCormac FG, Manning SW, Reimer RW, Richards DA, Southon JR, Talamo S, Turney CSM, van der Plicht J, Weyhenmeyer CE (2009) IntCal09 and Marine09 radiocarbon age calibration curves, 0-50,000 yeats cal BP. *Radiocarbon* 51(4):1111–1150.

86. Marks AE (1983) The Middle to Upper Paleolithic transition in the Levant. *Advances in World Archaeology* 2:123–136.

87. Hershkovitz I, Marder O, Ayalon A, Bar-Matthews M, Yasur G, Boaretto E, Caracuta V, Alex B, Frumkin A, Goder-Goldberger M, Gunz P, Holloway RL, Latimer B, Lavi R, Matthews A, Slon V, Bar-Yosef Mayer D, Berna F, Bar-Oz G, Yeshurun R, May H, Hans MG, Weber GW, Barzilai O (2015) Levantine cranium from Manot Cave (Israel) foreshadows the first European modern humans. *Nature* XXX doi:10.1038/nature14134

88. Bar-Yosef O, Arnold M, Mercier N, Belfer-Cohen A, Goldberg P, Housley R, Laville H, Meignen L, Vogel JC, Vandermeersch B (1996) The dating of the Upper Paleolithic layers in Kebara cave, Mt Carmel. *Journal of Archaeological Science* 23(2):297–306.

89. Barzilai O, Alex B, Boaretto E, Hershkovitz I, Marder O (2014) The Early Upper Palaeolithic at Manot Cave, Western Galilee, Israel. *PESHE* 3:34.

90. Szmidt CC, Normand C, Burr GS, Hodgins GW, LaMotta S (2010) AMS ^{14}C dating the Protoaurignacian/Early Aurignacian of Isturitz, France. Implications for Neanderthal-modern human interaction and the timing of technical and cultural innovations in Europe. *Journal of Archaeological Science* 37(4):758–768.

91. Douka K, Grimaldi S, Boschian G, Lucchese AD, Higham TF (2012) A new chronostratigraphic framework for the Upper Palaeolithic of Riparo Mochi (Italy). *Journal of Human Evolution* 62(2):286–299.

92. Schmidt C, Sitlivy V, Anghelinu M, Chabai V, Kels H, Uthmeier T, Hauck T, Băltean I, Hilgers A, Richter J, Radtke U (2013) First chronometric dates (TL and OSL) for the Aurignacian open-air site of Româneşti-Dumbrăviţa I, Romania. *Journal of Archaeological Science* 40(10):3740–3753.

93. Valoch K (2008) Brno-Bohunice, eponymous Bohunician site: new data, new ideas. *Man - Millennia - Environment. Studies in honour of Romuald Schild*, eds Sulgostowska Z, Tomaszewski AJ (Institute of Archaeology and Ethnology, Polish Academy of Sciences, Warsaw), pp 225–236.

94. Richter D, Tostevin G, Škrdla P (2008) Bohunician technology and thermoluminescence dating of the type locality of Brno-Bohunice (Czech Republic). *Journal of Human Evolution* 55(5):871–885.

95. Benazzi S, Douka K, Fornai C, Bauer CC, Kullmer O, Svoboda J, Pap I, Mallegni F, Bayle P, Coquerelle M, Condemi S, Ronchitelli A, Harvati K, Weber GW (2011) Early dispersal of modern humans in Europe and implications for Neanderthal behaviour. *Nature* 479(7374):525–528.

96. Trinkaus E, Milota S, Rodrigo R, Mircea G, Moldovan O (2003) Early modern human cranial remains from the Peştera cu Oase, Romania. *Journal of Human Evolution* 45:245–253.

97. Güleç E, Baykara I, Özer I, Sağır M, Erkman C (2007) Initial Upper Paleolithic human dental remains From Ucagizli Cave (Hatay, Turkey). *American Journal of Physical Anthropology* 132 (S44): 122

98. Douka K (2013) Exploring the great wilderness of prehistory: the chronology of the Middle to the Upper Paleolithic transition in the northern Levant. *Mitteilungen der Gesellschaft für Urgeschichte* 22:11–40

99. Sinitsyn AA (2003) The most ancient sites of Kostenki in the context of the Initial Upper Paleolithic of northern Eurasia. *The Chronology of the Aurignacian and of the transitional technocomplexes: dating, stratigraphies, cultural implications*, Trabalhos de Arqueologia, eds Zilhao J, d'Errico F (Instituto Português de Arqueologia, Lisboa), pp 89–107.

100. Haesaerts P, Damblon F, Sinitsyn A, Van der Plicht J (2004) Kostienki 14 (Voronezh, Central Russia): New data on stratigraphy and radiocarbon chronology. *Section 6: Le Paleolithique superieur / The Upper Palaeolithic: Sessions generales et posters / Gerneral sessions and posters, Acts of the XIVth UISPP Congress, University of Liege, Belgium, 2–8 September 2001*, BAR Int. Ser., eds Dewez M, Noiret P, Teheux E (Archaeopress), pp 169–180.

101. Marom A, McCullagh JSO, Higham TFG, Sinitsyn AA, Hedges REM (2012) Single amino acid radiocarbon dating of Upper Paleolithic modern humans. *Proceedings of the National Academy of Sciences USA* 109(18):6878–6881.

102. Sinitsyn AA (2003) A Palaeolithic 'Pompeii' at Kostenki, Russia. *Antiquity* 77:9–14.

103. Higham T, Ramsey CB, Karavanić I, Smith FH, Trinkaus E (2006) Revised direct radiocarbon dating of the Vindija G_1 Upper Paleolithic Neandertals. *Proceedings of the National Academy of Sciences USA* 103(3):553–557.

104. Hoffecker JF, Holliday VT, Anikovich MV, Sinitsyn AA, Popov VV, Lisitsyn SN, Levkovskaya GM, Pospelova GA, Forman SL, Giaccio B (2008) From the Bay of Naples to the River Don: the Campanian Ignimbrite eruption and the Middle to Upper Paleolithic transition in Eastern Europe. *Journal of Human Evolution* 55: 858–870.

105. Fu Q, Li H, Moorjani P, Jay F, Slepchenko SM, Bondarev AA, Johnson PLF, Aximu-Petri A, Prüfer K, de Filippo C, Meyer M, Zwyns N, Salazar-García DC, Kuzmin YV, Keates SG, Kosintsev PA, Razhev DI, Richards MP, Peristov NV, Lachmann M, Douka K, Higham TFG, Slatkin M, Hublin J-j, Reich D, Kelso J, Viola TB, Pääbo S (2014) Genome sequence of a 45,000-year-old modern human from western Siberia. *Nature* 514(7523): 445-449.

Chapter 4 · The Ksâr 'Akil chronology questioned

The paper that forms Chapter 3 (Bosch et al. 2015a) has been criticized by Douka et al. (2015). This chapter presents a short summary of their critiques and our published reply (Bosch et al. 2015b) as well as some additional remarks and suggestions as to how to move forward the debate on the chronology of Ksâr 'Akil.

4.1. Summary of Douka et al.'s critiques

Douka et al.'s (2015) criticisms revolve around two main points: (1) the way in which the Bayesian model was constructed; namely, they argue that it lacks consistent boundaries between phases and that we used incompatible approaches to determine the robustness of the model (i.e., using both agreement indices and outlier detection; and (2) they believe that our knowledge of the stratigraphy was inadequate.

The argumentation by Douka et al. (2015) is partly based on an inaccurate representation of our data set. For example, Douka et al. claim we did not build adequate boundaries into our model. Our boundaries in fact represent the archaeological layers and phases of the sequence as defined by the excavators (e.g., Ewing 1947) and by scholars who subsequently studied the material (for a summary, see Bergman and Goring-Morris 1987). However, excluding the lower boundary issue, to which is discussed below, the two models for the Ksâr 'Akil chronology presented by Douka et al. (2013) used the same amount of boundaries, especially in the lower part of the model where our age estimates diverge the most (Fig. 4.1). In other cases, they used even fewer, as their preferred model uses broader phases (e.g., MP, IUP) conflating—and mixing—the dates from different layers within a phase.